Metamorphic devolatilization, mineral reaction, and fluid alteration in the Mica Creek area (British Columbia, Canada) inferred from whole-rock and mineral nitrogen isotope signatures

by

Yingzhou Li

A thesis submitted in partial fulfillment of the requirements for the degree of

Master of Science

Department of Earth and Atmospheric Sciences
University of Alberta

Abstract

The Neoproterozoic Horsethief Creek Group metasedimentary rocks in the Mica Creek area (British Columbia, Canada) are an important supracrustal sequence in the Canadian Cordillera. They contain a continuous range of metamorphic grades from slate, progressively to schists in the biotite, garnet, kyanite zones, and gneisses in the sillimanite – K-feldspar zone. This metamorphic sequence provides an excellent opportunity to examine the behavior of nitrogen (N) in a collisional metamorphic environment, which has not been well studied to date. Our results show that, despite a large variation in N/K ratios, slates (N/K = 20.9 – 43.2, $\delta^{15}N$ = 4.1 – 6.0‰) and chlorite-zone phyllites (N/K = 19.1 – 64.7, $\delta^{15}N$ = 4.2 – 5.8‰) have relatively constant $\delta^{15}N$ values, which largely resemble the signature of the protolith. The biotite-zone schists show decreased N contents associated with increasing $\delta^{15}N$ values (N/K = 1.7 – 29.1, $\delta^{15}N$ = 9.9 – 14.8‰). This is consistent with metamorphic devolatilization of ^{15}N-depleted NH_3 at T < 500 ºC, resulting in ^{15}N enrichment in the biotite-zone schist. In contrast, the garnet-zone (N/K = 3.8 – 37.4, $\delta^{15}N$ = 8.1 – 9.6‰), kyanite-zone (N/K = 11 – 23, $\delta^{15}N$ = 7.2 – 9.2‰) and sillimanite – K-feldspar zone (N/K = 4.0 – 6.0, $\delta^{15}N$ = 7.1 – 8.1‰) samples show a trend of decreasing $\delta^{15}N$ values as well as N content relative to the biotite zone. This trend cannot be explained by the metamorphic devolatilization effect but is rather an isotopic alteration by a ^{15}N-depleted granitic melt and its associated fluid. A detailed look at the N isotope signatures of coexisting minerals in the metamorphic rocks shows that muscovite, biotite and plagioclase in some samples more or

less deviate from N isotope equilibrium fractionations, with $\delta^{15}N$ values of both plagioclase and muscovite being negatively correlated to those of biotite. This can be best explained by a kinetic isotopic effect associated with metamorphic reactions that use muscovite and plagioclase to produce biotite, suggesting that plagioclase has likely been involved in the metamorphic reactions.

Preface

All rock samples in this study were collected by the author on field trips to the Mica Creek area, BC in May 2017 and May 2018, with guidance of Drs. Tom Chacko and Long Li, and assistance from Dr. Jesse Reimink, Yuying Deng, Kan Li, Zhe Zhang, and Guangyan Zhou. The author was responsible for sample preparation (e.g. cutting, crushing and weighing), instrument establishment (for silicate N isotope analysis), data collection (nitrogen quantification and isotopic measurement in Dr. Long Li's Stable Isotope Geochemistry Laboratory at the University of Alberta) and the manuscript writing.

Acknowledgement

I would first like to express my sincere gratitude to my thesis supervisor Dr. Long Li of the Department of Earth & Atmospheric Science at the University of Alberta, for his consistent and generous support during my master study, and for his enthusiasm which has motivated me to pursuit further in the field of geology.

Secondly, I would like to thank Dr. Tom Chacko and Mark Labbe at the University of Alberta for their immense knowledge and valuable guidance throughout many stages of my study. This work would not be made possible without your help.

Thirdly, I would like thank Dr. Thomas Stachel for granting me access to the FTIR facility, Dr. Andrew Locock for his help on EPMA, and my colleagues Kan Li, Zhe Zhang, Yuying Deng for their crucial help throughout my research work.

Last but not the least, I would like to thank my parents for years of support and encouragement. I am forever in debt to them.

This research is generously funded by the Natural Sciences and Engineering Research Council of Canada.

Table of content

List of Tables

List of Figures

List of Abbreviations

All mineral abbreviations in this thesis follow those by Whitney and Evans (2010).

Ab =Albite	Ms = Muscovite
Bt = Biotite	Pl = Plagioclase
Chl = Chlorite	Qz = Quartz
Grt = Garnet	Sil-Kfs = Sillimanite – K-feldspar
Ilm = Ilimenite	Ky = Kyanite
Py = Pyrite	Sd = Siderite

1. Introduction

Nitrogen (N) exists virtually everywhere on this planet in different forms, including as N_2 gas, which makes up 78% of the present-day atmosphere, as NO_3^- and NH_4^+ in the hydrosphere (Sigman et al., 2009), and as reduced N in biosphere (Ader et al., 2006). In silicate minerals, N is a trace element and mostly resides as ammonium ion in the crystal lattice substituting for potassium and sodium ions because they have similar ionic radii and valences (Stevenson, 1959, 1962; Barker, 1964; Yamamoto and Nakahira, 1966; Honma and Itihara, 1981). In metamorphic and igneous rocks, NH_4^+ is most concentrated in biotite, followed in order by muscovite, K-feldspar and plagioclase (Honma and Itihara, 1981). Generally, in biotite and muscovite, the NH_4^+ concentration ranges from a few tens to more than a thousand parts per million (ppm) (Honma and Itihara, 1981; Duit et al., 1986; Haendel et al., 1986; Darimont et al., 1988).

Nitrogen isotope composition, coupled with variations of N content, have been used for tracing geological processes such as diagenesis, hydrothermal alteration, metamorphism, ore genesis and crust-mantle interaction (Duit et al., 1986; Haendel et al., 1986; Bebout and Fogel, 1992; Bebout, 1997; Ader et al., 1998; Jia and Kerrich, 1999). In particular, N behavior during metamorphic devolatilization has been a focus in previous studies of the geological N cycle. With enhanced metamorphic devolatilization, a general pattern of decreasing N content with increasing $\delta^{15}N$ value of whole rock has been widely observed in both subduction-related metamorphic sequences, such as the Catalina Schist in the USA (Bebout and Fogel, 1992) and the Erzgebirege schists in Germany (Haendel et al., 1986; Mingram and Bräuer, 2001), and collision-related regional metamorphic sequences, such as the Cooma metamorphic complex in Australia (Jia, 2006) and the Taiwan mountain belt in China (Yui et al., 2009). This pattern has

been explained as the result of progressive metamorphic devolatilization in which the light isotope (^{14}N) is preferentially lost, inducing continuous increase in the $^{15}N/^{14}N$ ratio of the residual N in the higher-grade metamorphic rocks (Duit et al., 1986; Haendel et al., 1986; Bebout and Fogel, 1992; Mingram and Bräuer, 2001). With laboratory experiments, Haendel et al. (1986) proposed that the magnitudes of N loss and consequent N isotope shift after metamorphism depend mainly on metamorphic temperature. During low-grade (greenschist-facies or lower) metamorphism, only about 5-7% of N is mobilized. In high-grade (upper amphibolite-facies or higher) metamorphism, up to 90% of original sedimentary N could be lost (Haendel et al., 1986). Similarly, in another study on the Catalina Schist, Bebout and Fogel (1992) found that the high-grade metamorphic rocks (amphibolite facies, ~650 ºC and ~1 GPa; Bebout, 1997) lost about 74% of the N relative to their protoliths. However, N behavior in the high-pressure (HP) to ultrahigh-pressure (UHP) metamorphic rocks in western Alps was very different. Busigny et al. (2003a) showed that N isotope composition of the Schistes Lustres Nappe did not show systematic change with increasing metamorphic conditions to at least 90 km depth (650ºC and ~3Gpa). Similarly, study of the N signatures of metasedimentary rocks of the Otago and Alpine Schists (New Zealand) also suggests minimal loss of nitrogen to lower amphibolite facies (Pitcairn et al., 2005). Based on this striking difference, geothermal gradient, rather than temperature solely, has been hypothesized to control the extent of metamorphic devolatilization (Busigny et al., 2003a). At low T/P conditions (a “cold slab”), such as the western Alps, metamorphic devolatilization could be limited, whereas at relatively high T/P conditions (a “warm slab”), such as the Catalina Schist, extensive devolatilization could occur.

For those terranes in which significant metamorphic devolatilization occur, the magnitude of N loss and associated N isotope shifts have been used to constrain the degassed N

species. For example, Bebout and Fogel (1992) observed an isotopic shift of 2.4‰ from lawsonite-albite grade to amphibolite equivalents. This magnitude of the shift fits into a isotopic fractionation between N_2 and NH_4^+, suggesting that N was released in form of N_2. Mingram and Bräuer (2001) illustrated a more complicated scenario with an isotopic shift of 5.5‰ from the low-grade unit to the gneiss/eclogite units, during which the modeled species of degassed N changed from NH_3 for garnet phyllite (~470 ºC) to N_2 for mica schists (~550 ºC), then back to NH_3 for garnet-phengite schist (>730 ºC). In a more recent study, Jia (2006) showed a much larger isotopic shift of 8.4‰ from sub-chlorite to sillimanite and migmatite zone. Such ^{15}N enrichment can be well explained by isotope fractionation between N_2 and NH_4^+ at 300-600 ºC followed by isotope fractionation between NH_3 and NH_4^+ at 650-730 ºC. The particular N species devolatilized may depend on the redox condition of the fluid as indicated by Duit et al. (1986) and Mikhail and Sverjensky (2014).

Compared with metamorphic effects in subduction-zone settings (Bebout and Fogel, 1992; Bebout, 1997; Busigny et al., 2003a; Halama et al., 2017), metamorphic reactions in collisional orogenic belts are expected to be more complicated because the thermal gradient may vary and large-scale external fluid may be involved (Rye et al., 1976; Ferry, 1988; Ague, 1991). However, the two studies of collisional belts mentioned above only reported a simple metamorphic devolatilization effect. The response of N to other factors in the collisional belt, such as external fluid and mineral reactions and their impact on the geological N recycling have not been reported.

The Barrovian metamorphic sequence of the souhtern Canadian Cordillera, which is considered to be representative of a collision-related orogenic belt, provides a natural laboratory to examine the N isotope behavior in a collisional metamorphic sequence. The metasedimentary

rocks of the Mica Creek area (British Columbia, Canada), which resulted from the Mesozoic to early Cenozoic crustal thickening, have been extensively studied in terms of their petrological and geochemical characteristics (Ghent et al., 1979; Ghent et al., 1980; Simony et al., 1980; Monger et al., 1982; Bowman and Ghent, 1986; Digel et al., 1998; Ghent and Valley, 1998; Crowley et al., 2000; Tinkham and Ghent, 2005). In one particularly relevant study, Bowman and Ghent (1986) examined the oxygen and hydrogen isotope ratios of several minerals (quartz, muscovite, biotite and ilmenite) in 12 rocks across the staurolite to sillimanite – K-feldspar (Sil-Kfs) zones and found that their $\delta^{18}O$ and δD values remain relatively constant both within individual metamorphic zones and across different zones. The homogeneities in hydrogen isotopes and oxygen isotopes were interpreted to be inherited from isotopically homogenous protolith (Bowman and Ghent, 1986), which implies that there was no significant metamorphic devolatilization and infiltration of external fluid during the regional metamorphism. If this is true, N isotope compositions of minerals and whole-rock samples are also expected to be relatively uniform.

In order to test this hypothesis, in this thesis, I investigated 23 samples from the Horsethief Creek Group metasedimentary rocks in the Mica Creek area. These samples are characterized by a medium P/T regional metamorphic sequence ranges from the sub-greenschist to upper-amphibolite facies. I report major- and trace-element compositions of whole rocks, major-element concentrations of muscovite and biotite, and N contents and isotope compositions of whole rocks as well as N-bearing minerals (e.g., biotite, muscovite, K-feldspar and plagioclase). In particular, to my knowledge, the N isotope data of K-feldspar and plagioclase have never been reported before in such sequences. These data provide new insights into

metamorphic devolatilization, fluid-rock interaction, and metamorphic reactions between minerals in an collisional metamorphic setting.

2. Geological Setting

2.1 Regional geological background

The Canadian Cordillera lies in the western edge of the North American Craton (Figure 1) and marks the western boundary of the Western Canadian Sedimentary Basin. Although the Canadian Cordillera is a relatively young mountain belt (~160 Ma), its sedimentary rocks has started to deposit in the Neoproterozoic in a miogeoclinal wedge along the western margin of the old North American Craton following episodic rifting of the Rodinia supercontinent (Monger and Price, 2002). Since the Jurassic (~185 Ma), the eastern Columbian Orogen, one of the two orogenic belts of the Canadian Cordillera, started to form as a result of compressional thickening of crustal rocks during collision between the North American plate and an accreted, composite, allochthonous terrane; the latter has been considered to be the magmatic arcs produced by subduction of the Pacific oceanic lithosphere beneath the old North American Craton prior to the collision (Monger et al., 1972; Dickinson, 1976; Monger et al., 1982). Around 60 Ma, the compressional regime of the area changed into crustal stretching and subsequent extensional deformation until ~40 Ma, resulting in major uplift, erosion and tectonic exhumation (Monger and Price, 2002).

The Canadian Cordillera is divided into five morpho-geological belts based on different sedimentology, mineralogy, metamorphic grade, structural style and geomorphology. From east to west, they are the Foreland, Omineca, Intermontane, Coast, and Insular belts (Figure 1) (Monger et al., 1972). High-grade rocks up to granulite facies and their partial melting product, granitic rocks, occur in the Coastal and Omineca belts, indicating that these rocks have been once buried to depth of >25 km (Monger and Price, 2002). Most exposed rocks in the flanking Foreland, Intermontane and Insular belts are sub-greenschist to greenschist facies at most and

have never been buried to more than 10 km (Monger and Price, 2002). The Omineca belt, as the metamorphic and plutonic hinterland to the Foreland belt, is dominated by Neoproterozoic to mid-Paleozoic miogeoclinal rocks, Precambrian basement rocks and Mesozoic plutonic rocks. The igneous intrusions were mainly emplaced in the Jurassic and Cretaceous, and affected by major compressional and/or extensional deformations in the early Tertiary (Monger et al., 1982; Monger and Price, 2002). Most of the rocks in the Omineca belt have been metamorphosed up to upper-most-amphibolite-facies conditions. Geothermobarometric studies on metapelites and amphibolites revealed that some of these rocks have experienced temperature more than 750 ºC and pressure near 8 kbar (Ghent et al., 1979; Stout et al., 1986; Farquhar, 1995; Ghent and Gordon, 2000; Tinkham and Ghent, 2005).

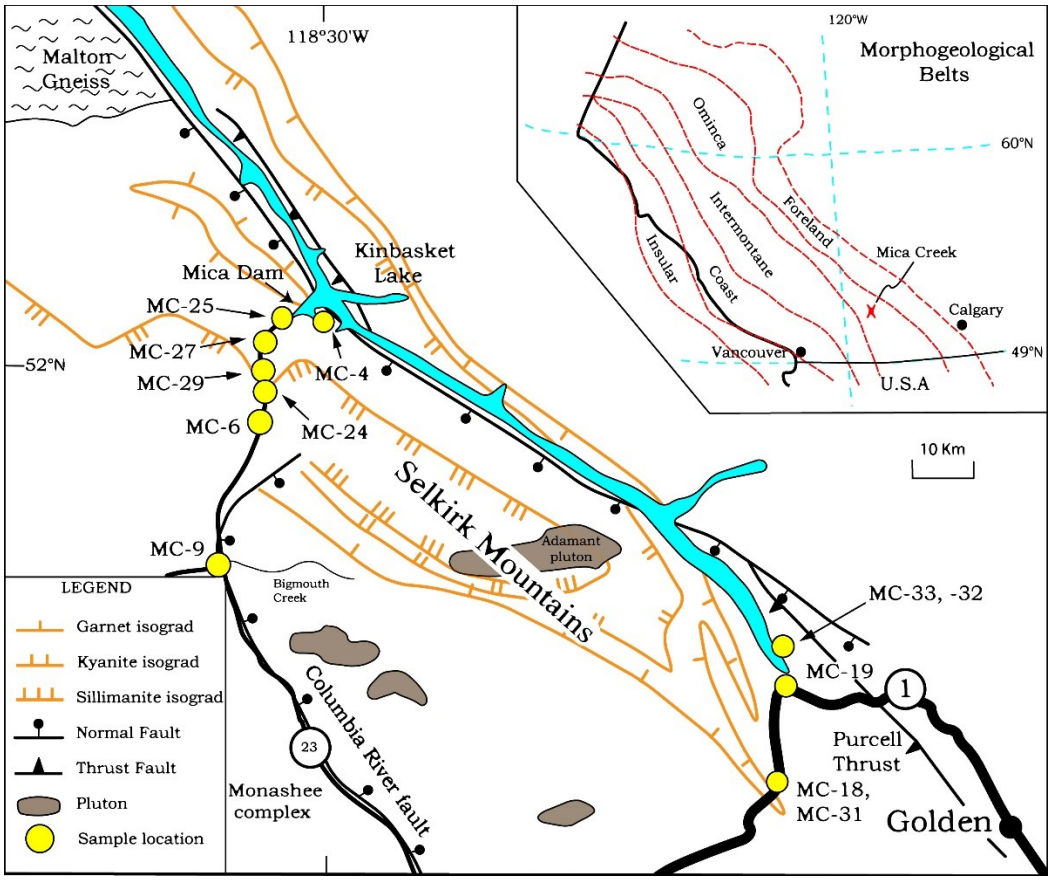

Figure 1. Geological sketch map of the Mica Creek area, BC (after Bowman and Ghent, 1986; Ghent and Gordon, 2000; Simony et al., 1980), showing metamorphic isograds and sample locations.

2.2 Geology of study area

The Mica Creek area is located in the southeastern Omineca belt (Figure 1). Over the last 40 years, there has been extensive study of the regional structural style, mineralogy, geochronology, and metamorphic conditions of rocks in the Mica Creek area (Ghent et al., 1979; Ghent et al., 1980; Simony et al., 1980; Bowman and Ghent, 1986; Stout et al., 1986; Ghent and Valley, 1998; Crowley et al., 2000; Ghent and Gordon, 2000; Tinkham and Ghent, 2005).

The Mica Creek area comprises mainly by a 5 km-thick succession of metasedimentary rocks known as the Neoproterozoic Horsethief Creek Group, together with minor igneous intrusions (~60 Ma) and Early Paleozoic strata (Lardeau and Hamill Group) to the south. Constrained by the presence of a broad staurolite-absent kyanite belt as the lower limit, and the lack of stable K-feldspar + kyanite as the upper limit (Simony et al., 1980; Crowley et al., 2000; Ghent and Gordon, 2000; Tinkham and Ghent, 2005), metamorphic pressures in the Mica Creek area correspond to bathozone 5 (6.5 to 7 kbar) of a typical Barrovian sequence (Carmichael, 1978). The metamorphic rocks of the Horsethief Creek Group cover the entire range from low-grade slate, chlorite-zone phyllite, biotite- and garnet-zone schists in the western Rockies and west of the Purcell Thrust to kyanite-zone schist and Sil-Kfs-zone gneiss in the Northern Selkirk mountain (Ghent et al., 1979; Simony et al., 1980; Bowman and Ghent, 1986; Ghent and Gordon, 2000). Despite the occurrence of various lithologies (e.g., pelites, semipelites, amphibolites, carbonates, and calc-silicate rocks) in the Horsethief Creek Group, a relatively consistent stratigraphic succession is retained throughout the area, which provides the confidence to trace the strata and infer its protolith (Ghent and Gordon, 2000).

Based on monazite U-Pb dating, five major thermo-tectonic events have been identified to occur at 163, 122, 110, 99-93 and 72-58 Ma, which roughly coincided with the five major

orogenic periods in the southeastern Canadian Cordillera (Crowley et al., 2000). Three major phases of deformation, although not geochronologically determined, have affected the rocks of this area. Phase 1 deformation produced the southwest-verging recumbent folds, which were then refolded into smaller-scale, northeast-verging, open to isoclinal folds (Phase 2), and lately refolded again into more open folds (interlimb angles range from 120º to 70º) with axial surfaces generally dipping southwest (Phase 3) (Ghent et al., 1977; Simony et al., 1980). The dominant schistosity in the Mica Creek area is a combination of Phase 1 and 2 axial plane structures, which can hardly be distinguished from each other, and thus referred as S_{1+2} (Simony et al., 1980; Raeside and Simony, 1983; Ghent and Gordon, 2000). It is commonly accepted that the peak metamorphism took place in late Phase 2 deformation and predated the Phase 3 folding event. This is supported by the observations that (i) kyanite and other major minerals have grown across S_{1+2} and have been bent and kinked by Phase 3 deformation, and (ii) the isograd surfaces have been deflected by Phase 3 folds (Craw, 1978; Ghent and Gordon, 2000). Although Phase 3 deformation is large in scale and intensive in some local areas, it produced little retrograde metamorphism and allowed peak metamorphic mineral assemblage to be preserved (Ghent and Gordon, 2000).

3. Sample Description

The sampling strategy for this study was to collect metapelitic rocks of the Horsethief Creek Group over a range of metamorphic grades. Samples close to late igneous intrusions are not included in this study to avoid the potential complication effects of magmatic fluid infiltration. A total of 23 metapelitic samples were collected from road cuts in the south of the Kinbasket Lake along two transects along Highways 23 and 1 (Figure 1) covering a continuous metamorphic sequence from sub-greenschist to upper amphibolite facies (except for the staurolite zone, which was not found in the field). The total sampling area spans approximately 150 km^2. Thin sections were made of all representative samples to examine mineral assemblages and determine metamorphic grade. The representative mineral assemblages and their corresponding metamorphic zones are listed in Table 1. Detailed observations on both hand samples and thin sections are summarized below.

MC-18-1, MC-31-1, MC-31-2 (~7 km south of the east gate of the Glacial National Park of Canada along Highway 1), and MC-33-1 (1.5km north of Beaver): These are slates containing ferroan carbonate (most likely siderite), quartz, muscovite and rare chlorite (Figure 2A). It is relatively easy to identify and trace the bedding planes formed prior metamorphism and crenulation cleavages, as well as the metamorphic foliations (with some efforts) in these samples. These are the lowest grade samples in this study and they closely resembles the protolith of the Horsethief Creek Group metasedimentary rocks.

Table 1. Characteristics of metamorphic zones and mineral assemblages for the Horsethief Creek Group metasedimentary rocks.

Zone	Metamorphic grade	P-T condition*	Lithology	Mineral assemblage
Low-grade	Sub-greenschist facies	-	Slate	Ms + Qz +Py + Sd
Chlorite	Greenschist facies	-	Phyllite	Chl + Ms +Qz
Biotite	Upper greenschist facies	-	Schist	Bt+ Ms + Qz + Pl ± Chl
Garnet	Amphibolite facies	5-7 kbar; 480~625°C	Schist	Grt + Bt + Ms + Qz + Pl
Kyanite	Amphibolite facies	6.1 ± 0.8kbar; 625 ± 27°C	Schist	Ky + Bt + Ms + Grt + Qz + Pl ± Kfs
Sillimanite – K-feldspar	Amphibolite facies	7.2 ± 0.8kbar; 696 ± 27°C	Gneiss	Bt + Ms + Qz + Pl + Kfs

* Metamorphic pressure and temperature data are from Craw (1978), Ghent (1982) and Farquhar (1995).

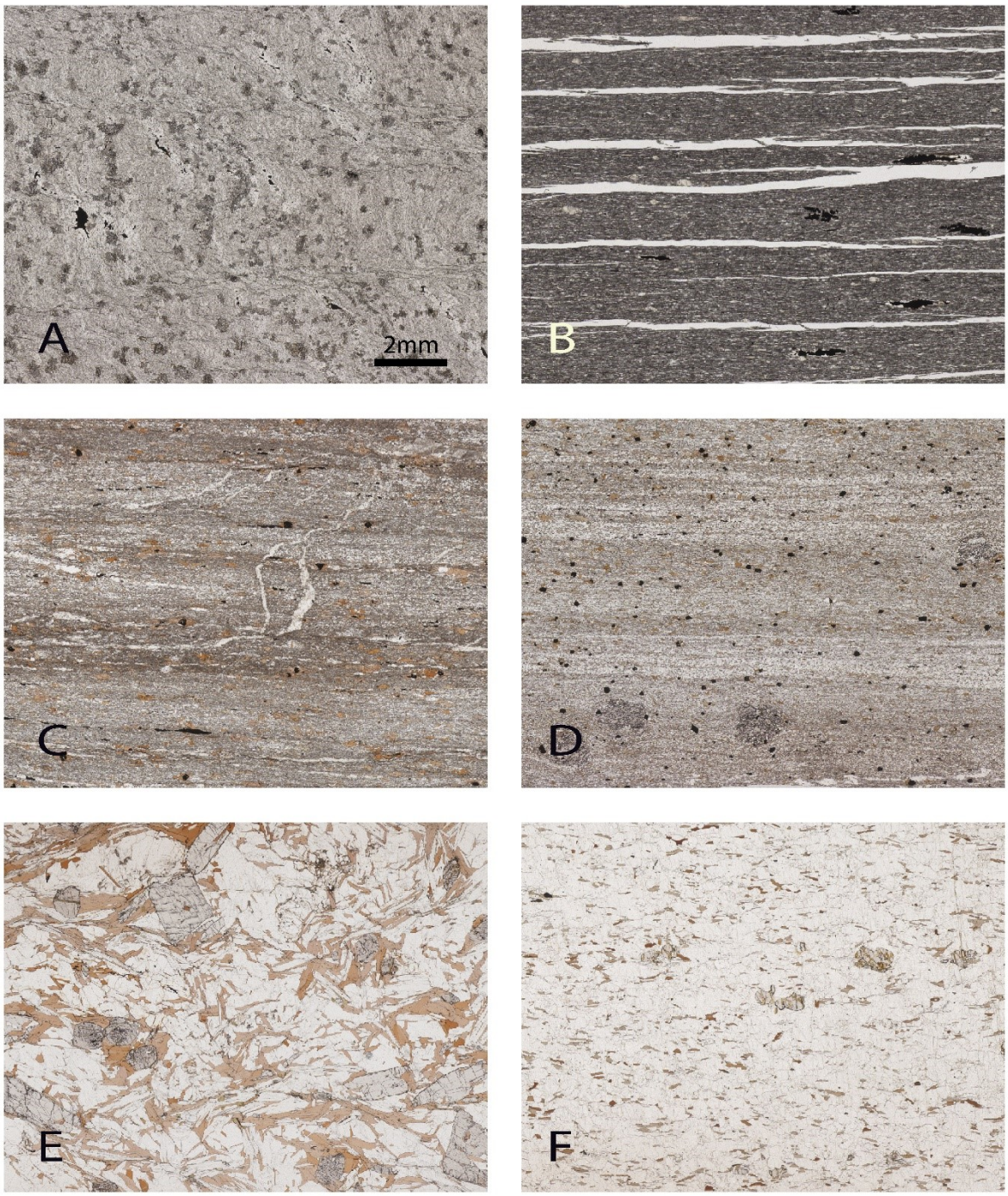

Figure 2. Thin section photographs of representative samples from each metamorphic zone of the Horsethief Creek Group metasedimentary rocks. A: MC-18-1, low-grade slate; B: MC-19-1, chlorite-zone phyllite; C: MC-9-3, biotite-zone schist; D: MC-9-1, garnet-zone schist; E: MC-4-4, kyanite-zone schist; F: MC-6-6, sillimanite – K-feldspar -zone gneiss. The scale bar is presented in A and the same for all other graphs.

MC-19-1, MC-19-2, MC-32-1, MC-32-2 (~11km north of the east gate of the Glacial National Park of Canada along the Highway 1): These are phyllite samples containing calcite, chlorite, muscovite and abundant visible magnetite with grain size ranging from 0.7 mm to 3 mm (Figure 2B). The magnetite grains are commonly associated with hematite rust. These samples belong to lower-greenschist facies and are classified into the chlorite zone based on the presence of chlorite and absence of biotite.

MC-9-2, MC-9-3, MC-9-4, MC-27-1 (~17.5 km north of Goldstream Creek, roadcut along Highway 23): These schist samples consist of biotite, muscovite, plagioclase and quartz, and minor chlorite and ilmenite, with local calcite and dolomite veins (Figure 2C). These are typical biotite-zone samples with relatively well-developed schistosity. Biotite and muscovite have a relatively constant grain size of <0.7mm. Carbonate veins are conspicuous in MC-9-3. These veins vary from 0.1 mm to 0.7 mm in width, and occur both along and across foliations, suggesting late formation. Dark reaction zones (~0.2mm) occur commonly between these carbonate veins and the host rocks. Quartz and plagioclase are particularly abundant in MC-9-2. Minor chlorite alteration of biotite in MC-9-2 and MC-9-4 suggest that retrograde alteration has taken place.

MC-9-1 (~4 metres from MC-9-2); MC-25-1, MC-29-1 (south of the Mica Creek Town): These samples are schists that are composed of biotite, garnet, muscovite, ilmenite with rare chloritoid (Figure 2D). Based on the mineralogy, they belong to the garnet zone. These samples are very similar to MC-9-2, -3 and -4 in term of texture and grain size except for presence of garnet porphyroblasts. Garnet grains range from 1.4 mm to 2 mm in diameter and exhibit an extensive poikiloblastic texture. Based on the presence of pressure shadow, wrapping fabric and curved inclusion trails inside garnet, these garnets are considered to be syn-tectonic. There are no

vein observed in both hand samples and thin sections. These samples show much less retrogression than MC-9-2, -3 and -4. The close spatial distribution of the four MC-9 samples (Figure 1) implies that they should have experienced similar pressure and temperature conditions. The presence of garnet in MC-9-1 is probably due to the difference in bulk composition (e.g. MC-9-1 is more Al-, Fe- and Mg-rich than MC-9-2, -3, -4).

MC-4-1, MC-4-2, MC-4-3, MC-4-4, MC-4-5, MC-4-6: (from south shore of the Kinbasket Lake): These samples are schists composed of biotite + kyanite + garnet ± muscovite ± K-feldspar with minor tourmaline, and rare ilmenite (Figure 2E). Such a mineral assemblage indicates that these samples have kyanite zone assemblage and have not passed the sillimanite-in isograd. This observation is congruent with those of Tinkham and Ghent (2005) and Digel et al. (1998). The schistosity is well developed and defined by the uniform orientation of both biotite and muscovite. Subhedral to euhedral kyanite porphyroblasts range from 1.3 mm to 15.6 mm in length (along c-axis), and garnet poikiloblasts range from 0.7 mm to 4.7 mm in diameter. The schistosity is typically deflected around kyanite and garnet porphyroblasts and forms a wrapping texture with or without pressure shadow. Along with internal fabric defined by the curvy inclusion trails of garnet, it is evident that garnets and kyanites are syn-tectonic. Kyanite prophyroblasts are typically aligned with schistosity. Biotite and muscovite have sharp grain boundaries. These rocks are not migmatized nor is there any significant retrogression of the primary mineral assemblage.

Quartz-feldspar (granitic) veins at various size (0.2 to 3cm in width) are observed in some outcrops at this locality (Figure 3). No reaction rim is found between the veins and wall rock. Some veins have been truncated by the growth of kyanite and garnet. The veins, together

with kyanite, align in parallel to the foliation. These observations suggest that the veins were formed no later than the peak metamorphism.

MC-6-6 and MC-6-7 (~3.8 km south of the Mica Creek Town): These gneisses represent the highest-grade (Sil-Kfs zone) samples collected in this study (Figure 2F). They are quartz- and feldspar-rich gneisses characterized by a mineral assemblage of biotite + garnet + K-feldspar + muscovite. All mica grains (<1 mm) are significantly smaller than the ones in the kyanite-zone samples. The absence of aluminosilicate minerals is possibly attributed to the retrograde reaction such as Als + Kfs + H_2O → Ms + Qtz, which consumed all the aluminosilicates. As such, the muscovite is not part of the peak temperature metamorphic assemblage.

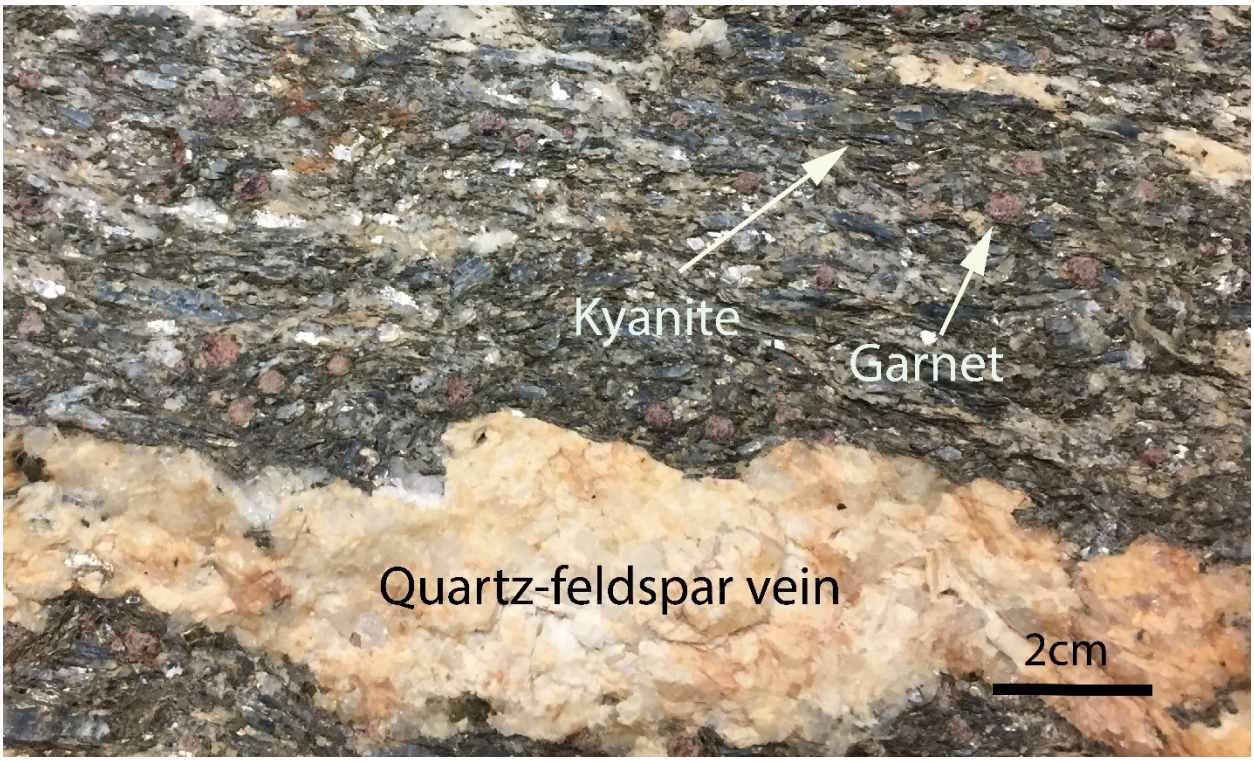

Figure 3. Photograph of the quartz-feldspar vein in a kyanite-zone sample.

4. Methodology

4.1 Whole-rock major- and trace-element analyses

Whole-rock major- and trace-element concentrations were measured at the Activation Laboratories Ltd. in Ontario, Canada. Whole-rock sample > 1kg was crushed and ground to <200 mesh in an agate mortar. A small quantity (~0.2 g) of sample powder is mixed with lithium metaborate/lithium tetraborate in a graphite crucible and fused in an induction furnace at 1150 ºC. The molten mixture is then poured into a 5% nitric acid solution and shaken for ~30 min to be fully dissolved. The major- and trace-element concentrations were measured on a simultaneous/sequential Thermo Jarrell-Ash ENVIRO II ICP or a Varian Vista 735 ICP. Calibration was achieved using 7 USGS and CANMET certified reference materials. The analytical uncertainty (1σ) is 0.5-5% for major elements depending on concentration and 10% for trace elements relative to their absolute contents.

4.2 Major elements of mica minerals

To examine the chemical variability of minerals across metamorphic grades, 45 muscovite and 45 biotite (5 grains per sample) from the chlorite (5 muscovite), biotite (10 muscovite and 10 biotite), kyanite (20 muscovite and 25 biotite) and Sil-Kfs (10 muscovite and 10 biotite) zones were selected for major-element analysis by Electron probe microanalysis (EPMA). For each muscovite or biotite grain, three spots were measured to examine the inner-grain variability.

EPMA analysis was undertaken with a Cameca SX100 in the Electron Microprobe Laboratory at the University of Alberta using wavelength dispersive spectrometry (WDS). The

analyses were done with 20kV accelerating voltage, a beam current of 20 nA and a beam size of 5 microns. The following mineral standards were used in the analyses: synthetic Rutile for Ti, $NaAlSi_3O_8$ Albite for Na, Gore Garnet for Si, Spessartine for Mn and Fe, Frank Smith Pyrope Garnet for Mg and Al, Wakefield Diopside for Ca. The precision of the EPMA analyses are ~1% relative for elements at >10 wt.% concentration, ~2-5% relative for elements at 1-10 wt.% concentration and 5-10% relative for elements at 0.1-1 wt.%.

4.3 Nitrogen content and isotopic analysis of whole rocks and mineral separates

N isotope composition is expressed as:

$$\delta^{15}N = \left\{\left[\left({}^{15}N/{}^{14}N\right)_{sample}/\left({}^{15}N/{}^{14}N\right)_{standard}\right] - 1\right\} \times 1000 \quad (1)$$

where the standard is atmospheric N_2. The N content and isotope compositions were analyzed in a custom-made manifold (Figure 4) for quantification and isotopic measurement of nanomolar N_2 in the Stable Isotope Geochemistry Laboratory at the University of Alberta. The method employed a sealed-tube combustion technique similar to Li et al. (2014) and an offline extraction technique coupled with helium gas to transfer the N_2 gas to an isotope-ratio mass spectrometer (IRMS) for isotopic analysis, which is similar to the method developed by Bebout et al. (2007). The detailed method is described below.

Mineral (micas and feldspars) or whole-rock samples were ground into fine powder (<200 mesh) by a pestle and an agate mortar. A sample was then loaded together with CuO into a pre-cleaned quartz tube (at 1000°C for 2 hours), which was then pumped overnight and sealed by a torch under high vacuum. The sealed sample tubes were combusted at high temperatures to release N. The combustion temperature and duration vary from mineral to mineral (see explanation below and Table 2). After this step, the sealed tube was then put in a programmable

muffle furnace at 1000ºC for 8 hours to ensure complete release of N from minerals and rocks, followed by slow cooling to 600°C. The tubes were then held at 600°C for 2 hours before further cooling down to room temperature so as to ensure the reduction of oxidized N species to N_2, which is the working gas for mass spectrometer analysis.

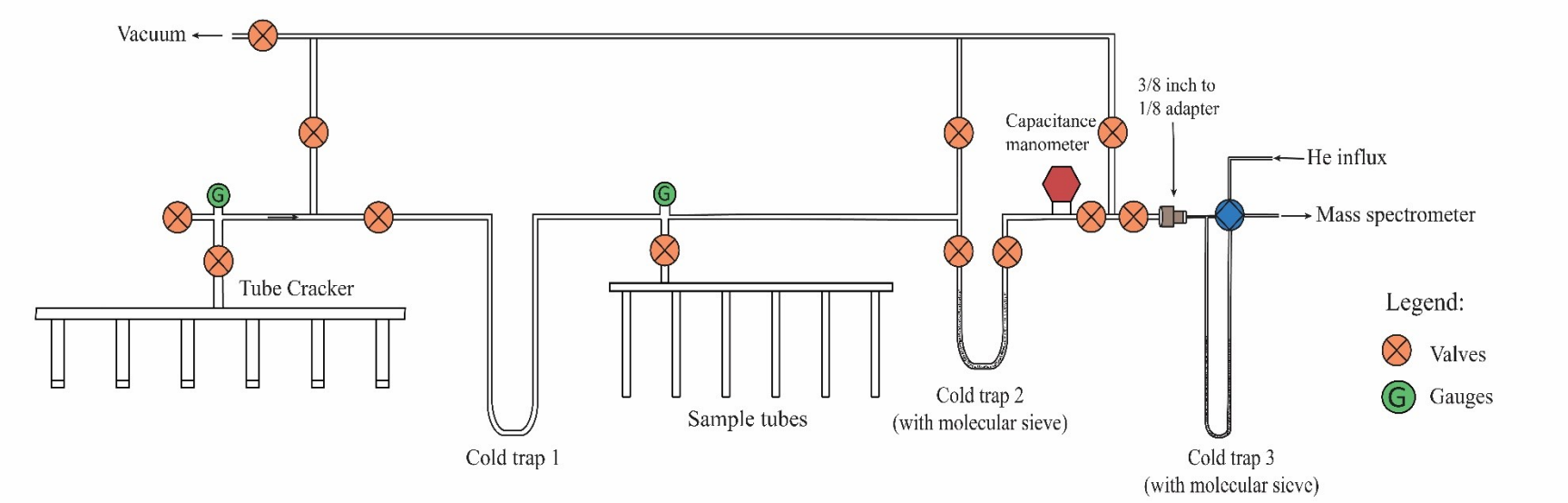

Figure 4. Schematic illustration of the high-vacuum line and carrier-gas system at the Stable Isotope Geochemistry Laboratory of the University of Alberta (modified from Bebout et al., 2007).

Regarding the combustion temperature and duration for N release from minerals, Sadofsky and Bebout (2000) demonstrated that N can be completely released from muscovite at 1000 ºC overnight whereas N release from biotite requires extra combustion at a higher temperature of 1200 ºC for 30 min. However, the appropriate combustion temperatures for K-feldspar and plagioclase have not been examined before. To determine the appropriate combustion temperature and duration for N extraction from these two minerals, I compared the N contents and isotope compositions from combustion at a variety of temperatures (Table 2; Figures 5 & 6). The results indicate that, for K-feldspar, an extra combustion at 1200 ºC for 30 min gave the best yield and reliable isotope compositions (Figure 5); combustion at 1100 ºC for 30 min gave similar isotope compositions within error but much lower content, whereas over combustion at 1200 ºC for 60 min gave lower content with higher $\delta^{15}N$ values (Table 2; Figure 5). This over-combustion effect has also been observed, to a lesser extent, for micas (Sadofsky and Bebout, 2000) and altered oceanic crust (Li et al., 2007). We speculate that some N might dissolve back into the mineral while some unknown reaction or melting occurs at high temperatures. For plagioclase, the results (Figure 6) show combustion at 1200 ºC for 60 min is required for the N release to yield reliable concentration and isotopic data.

Table 2. Released N and its $\delta^{15}N$ value at different combustion temperatures and durations for K-feldspar and plagioclase.

Sample ID	Combustion temperature and duration	N released (ppm)	$\delta^{15}N$ (‰)
MC-6-7 K-feldspar			
	1000 ºC for 8 h	53.8	8.0
	1100 ºC for 30min + 1000 ºC for 8 h	64.1	8.8
	1100 ºC for 30min + 1000 ºC for 8 h	67.6	8.7
	1200 ºC for 30min + 1000 ºC for 8 h	104.0	9.0
	1200 ºC for 30min + 1000 ºC for 8 h	108.5	9.1
	1200 ºC for 60min + 1000 ºC for 8 h	95.7	9.6
	1200 ºC for 60min + 1000 ºC for 8 h	91.6	9.4
MC-6-7 plagioclase			
	1000 ºC for 8 h	25.3	5.8
	1000 ºC for 8 h	24.2	5.3
	1100 ºC for 30min + 1000 ºC for 8 h	27.3	6.4
	1100 ºC for 30min + 1000 ºC for 8 h	27.2	6.5
	1200 ºC for 30min + 1000 ºC for 8 h	28.9	6.6
	1200 ºC for 30min + 1000 ºC for 8 h	27.9	6.4
	1200 ºC for 60min + 1000 ºC for 8 h	28.7	7.0
	1200 ºC for 60min + 1000 ºC for 8 h	29.0	6.7
MC-6-6 plagioclase			
	1000 ºC for 8 h	37.4	7.0
	1000 ºC for 8 h	32.3	6.8
	1100 ºC for 30min + 1000 ºC for 8 h	41.5	7.3
	1100 ºC for 30min + 1000 ºC for 8 h	46.5	7.8
	1200 ºC for 30min + 1000 ºC for 8 h	55.6	8.3
	1200 ºC for 30min + 1000 ºC for 8 h	57.9	8.7
	1200 ºC for 30min + 1000 ºC for 8 h	59.6	8.4
	1200 ºC for 60min + 1000 ºC for 8 h	65.0	8.8
	1200 ºC for 60min + 1000 ºC for 8 h	65.6	8.7
	1200 ºC for 90min + 1000 ºC for 8 h	63.7	8.8
	1200 ºC for 90min + 1000 ºC for 8 h	66.8	8.9

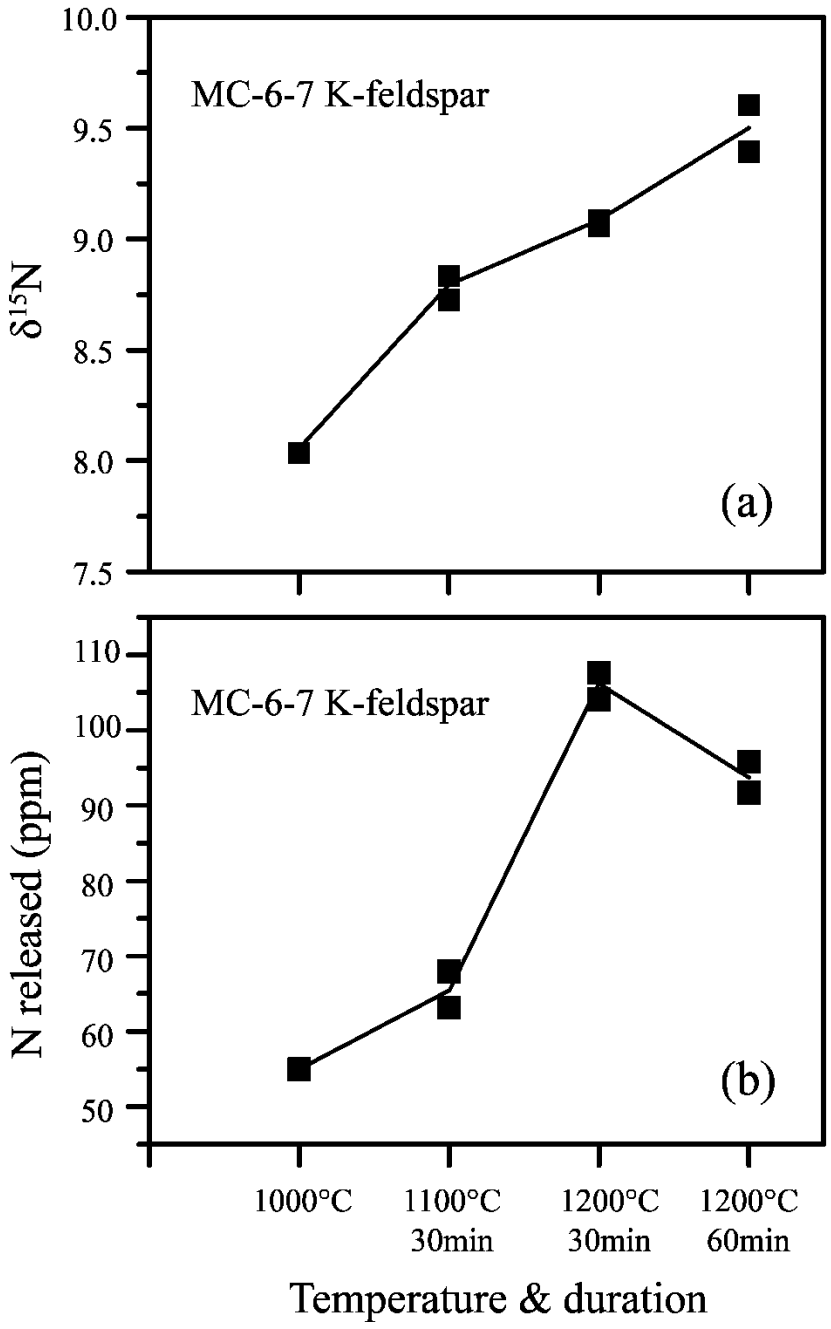

Figure 5. Isotope compositions (a) and contents (b) of N released from K-feldspar at different combustion temperatures and durations. See Table 2 for numerical data and text for detailed method.

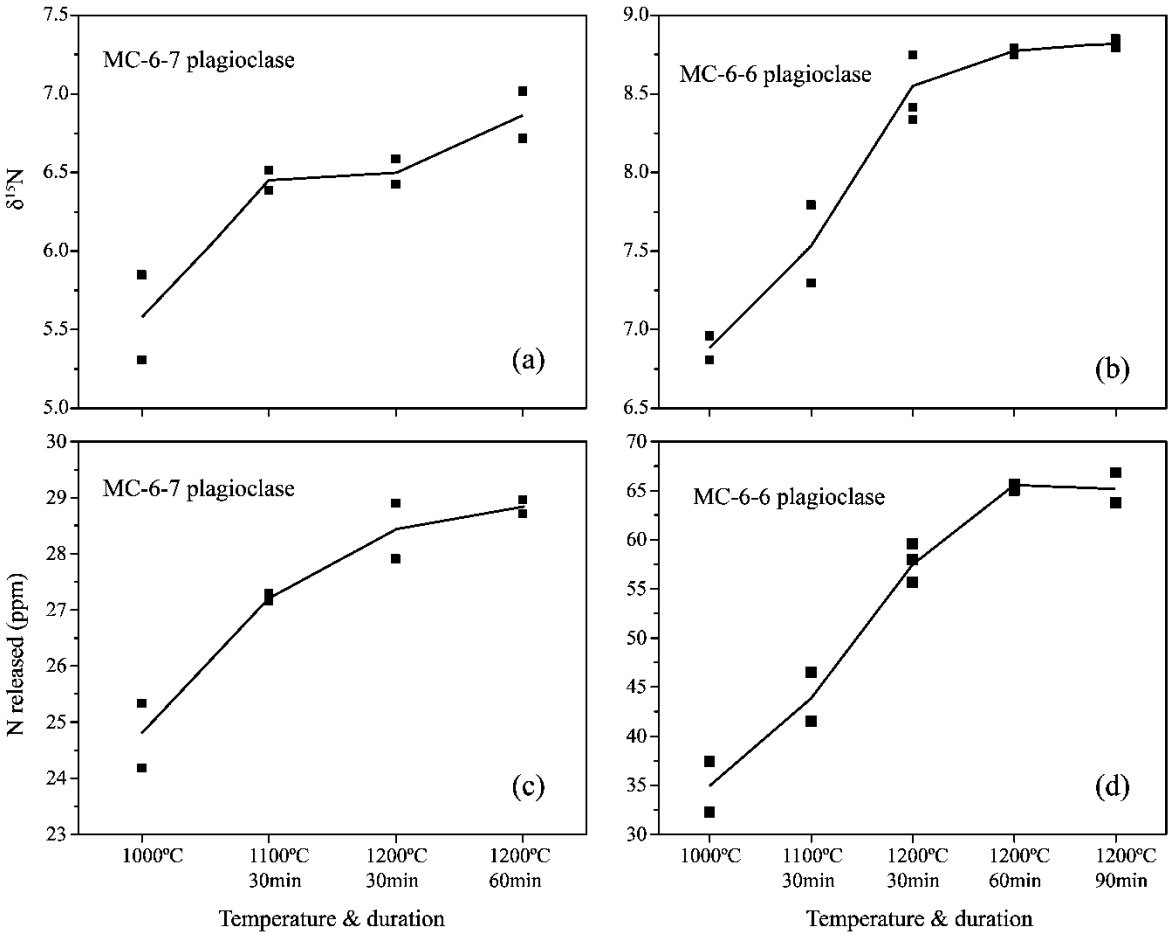

Figure 6. Isotope compositions (a&b) and contents (c&d) of N released from two plagioclase samples (MC-6-6 & MC-6-7) at different combustion temperatures and durations. See Table 2 for numerical data and text for detailed method.

After combustion, the sample tubes were put into a sample cracker in the custom-made extraction line (Figure 4), which was then pumped overnight to high vacuum. The sample tube was then broken to release the produced gases (N_2, H_2O, Ar, $\pm CO_2$, $\pm SO_2$) from combustion. Condensable gases were removed by liquid nitrogen in a cold trap (Cold trap 1 in Figure 4) and the remaining N_2 was concentrated into a fix volume by a cold trap with molecular sieve (Cold trap 2 in Figure 4) for quantification by a capacitance manometer. Finally, the N_2 was sent by a

helium stream through a Gasbench II interface to an IRMS (Fischer MAT 253) for isotopic measurements. The helium flow ensures the separation of N_2 from any other small amount of remaining incondensable gas (e.g., Ar). Another focus of N_2 using a cold trap with molecular sieve was applied in the Gasbench II system right before the transfer of N_2 to the IRMS to optimize the peak shape. Based on the results of repeated analyses of three reference materials (see Figure 7) and samples over the course of this study, this carrier-gas system has been demonstrated to be able to precisely measure extremely low amounts of N_2 (as small as 50 nmol) with small uncertainty ($1\sigma < 5\%$ of the N concentration and $< 0.2‰$ for $\delta^{15}N$).

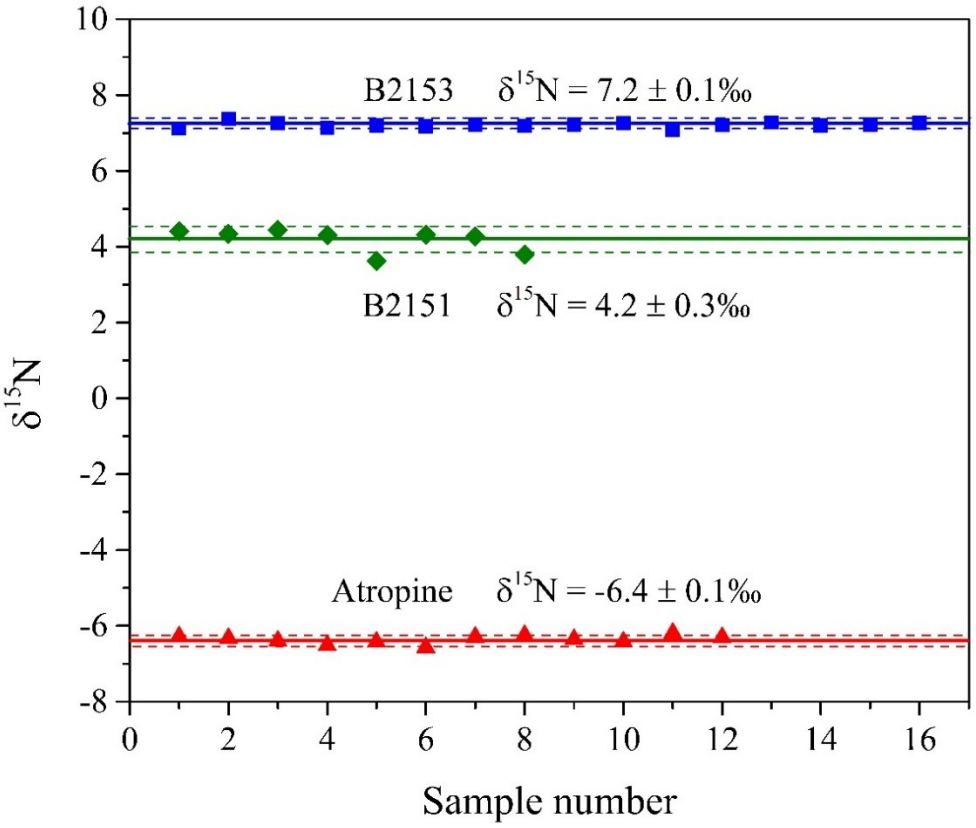

Figure 7. Results of N isotope measurements of three reference materials. The standard deviations shown are 1σ. B2153 is a low organic soil reference material with recommended $\delta^{15}N = 6.97 \pm 0.13‰$.

B2151 is a high organic sediment reference material with recommended $\delta^{15}N = 4.32 \pm 0.20‰$. Atropine is an organic reference material with recommended $\delta^{15}N = -6.3 \pm 0.1‰$.

4.4 Nitrogen content of muscovite measured by Fourier-transform infrared spectroscopy

For comparison, I also measured the N contents of selected muscovite samples by the Fourier-transform infrared spectroscopy (FTIR) technique following Busigny et al. (2003b). For each sample, about 10 single grains were measured in the FTIR facility (Nicolet) in the De Beers Laboratory for Diamond Research at the University of Alberta. The conditions of spectra acquisition include a resolution of 4 cm^{-1} and a scan number of 200. The beam size was adjusted to 50 μm. In order to avoid diffraction, all analyses were performed with beam directions parallel to the c-axis (perpendicular to <001> crystallographic direction).

Busigny et al. (2003b) derived an equation from the Beer-Lambert law, which predicts the relationship between grain thickness and the IR absorbance of major molecular species (e.g. SiO_4^{4-}). According to Busigny et al. (2003b), the absorbance difference between 1282 and 2514 cm^{-1} produces best result after numerous tests on random wave numbers. The formula for unpolished muscovite grains is:

$$d_{muscovite} = 119.38 * (A^{1282} - A^{2514}) \quad (2)$$

where $d_{muscovite}$ is the thickness of muscovite grain. A^{1282} and A^{2514} are the absorbance peak areas measured for wave numbers of 1282 and 2514 cm^{-1}, respectively. In addition, the Beer-Lambert law predicts a linear relationship between ammonium concentration of muscovite and the ratio of ammonium absorbance over muscovite thickness. Busigny et al. (2003b) constrained the parameters for the relationship as:

$$[NH_4^+] \text{ (ppm)} = 13.4 * ((A^{1430} - A^{2514}) / \text{thickness (cm)}) - 606 \quad (3)$$

where [NH_4^+] is the concentration of ammonium in parts per million. A^{1430} and A^{2514} are absorbance peak areas of wave numbers of 1430 and 2514 cm^{-1}, respectively.

5. Result

5.1 Whole-rock major and trace elements

The major- and trace-element concentrations of whole rocks are listed in Tables 3 and 4. Metasedimentary rocks of the Horsethief Creek Group from six metamorphic zones are characterized by a wide range of SiO_2 (49.5 to 80.4 wt%), Al_2O_3 (10.1 to 23.3 wt%), and K_2O (1.2 to 4.87 wt%) contents (Table 3). While these contents in each zone are relatively homogeneous, SiO_2 varies from 57.2-64.8 wt% in low-grade slate to 71.1-80.4 wt% in Sil-Kfs gneiss, Al_2O_3 varies from 13.3-23.2 wt% in low-grade slate to 10.1-14.8 wt% in Sil-Kfs gneiss, K_2O varies from 2.5-4.5 wt % in low-grade slate to 2.9-4.7 in Sil-Kfs gneiss. There is no systematic change in major-element compositions with progressive metamorphism. The LOI contents and the LOI/Al_2O_3 ratios decrease by a factor of 7.2 from low-grade slate (~5.57 wt%) to Sil-Kfs zone gneiss (0.78 wt%). Rb and Cs concentrations across the six metamorphic zones also display wide ranges from 53 to 226 ppm and 2.3 to 13.6 ppm respectively with no systematic change (Table 4).

5.2 Major element concentrations of mica minerals

The major-element compositions of biotite and muscovite grains are listed in Table 5 and plotted in Figure 8. Biotite grains (total n = 9) from the biotite, kyanite and Sil-Kfs zones are characterized by relatively uniform concentrations of K_2O and Al_2O_3, ranges from 8.87 to 9.67 wt% ($1\sigma = 0.3$) and from 18.97 to 20.5 ($1\sigma = 0.5$), respectively. In contrast, MgO contents of these biotite grains show large variations range from 10.02-10.14 wt% in biotite zone to 6.91-6.99 wt% in Sil-Kfs zone. Total Fe contents (expressed as FeO) of biotite also show large

variation range from 18.16 - 18.78 wt% in biotite zone to 20.68 - 20.97 wt% in Sil-Kfs zone. The higher FeO and lower MgO contents of Sil-Kfs-zone gneiss compared to biotite- and kyanite-zone schists are possibly due to Fe-Mg exchange between biotite and garnet. As temperature gets higher, garnet becomes more Mg-rich and biotite become more Fe-rich (Ferry and Spear, 1978). Muscovite grains (total n = 9) from chlorite, biotite, kyanite and Sil-kfs zones have K_2O contents from 9 to 11.2 wt% ($1\sigma = 0.7$), Al_2O_3 contents from 34.85 to 36.91 wt% ($1\sigma = 0.5$), FeO contents from 0.99 to 1.79 wt% ($1\sigma = 0.3$) and MgO contents from 0.65 to 1.35 wt% ($1\sigma = 0.2$).

Table 3. Whole-rock major element compositions (in weight percent) of the Horsethief Creek Group metasedimentary rocks.

Sample ID	SiO_2 (wt%)	Al_2O_3	Fe_2O_3(T)	MnO	MgO	CaO	Na_2O	K_2O	TiO_2	P_2O_5	LOI	Total
Low-grade												
MC-18-1	64.8	14.0	6.4	0.0	2.6	0.3	0.4	4.2	0.7	0.1	6.7	100.1
MC-31-1	60.28	17.22	11.58	0.151	0.41	0.15	1.15	3.34	0.811	0.16	5.25	100.5
MC-31-2	57.19	13.34	18.3	0.253	0.46	0.14	1.01	2.53	0.728	0.18	6.21	100.3
MC-33-1	57.29	23.19	6.76	0.045	2.15	0.1	0.87	4.53	0.829	0.09	4.17	100
Chlorite zone												
MC-19-1	50.0	19.2	8.7	0.1	2.7	4.9	1.1	3.6	0.9	0.1	8.1	99.3
MC-19-2	55.3	15.5	7.6	0.1	2.6	4.1	0.7	3.6	0.7	0.1	8.2	98.5
MC-32-1	55.61	21.05	10.65	0.059	3.17	0.09	1.97	3.35	0.892	0.07	3.97	100.9
MC-32-2	54.92	21.12	9.77	0.059	2.9	0.21	1.81	3.73	0.83	0.15	3.98	99.49
Biotite zone												
MC-9-2	70.5	10.5	3.8	0.0	1.1	5.3	2.6	1.2	0.6	0.1	4.3	99.9
MC-9-3	54.9	16.4	6.6	0.1	2.3	8.0	1.6	3.5	0.8	0.2	6.2	100.6
MC-9-4	57.2	13.4	5.9	0.2	1.8	11.0	1.4	1.9	0.9	0.1	6.6	100.2
MC-27-1	55.54	17.01	9.11	0.117	5.34	2.59	2.13	4.87	1.38	0.34	1.23	99.66
Garnet zone												
MC-9-1	61.22	18.73	7.57	0.042	2.37	1.17	2.09	4.09	1.176	0.15	2.08	100.7
MC-29-1	61.51	14.53	9.59	0.087	4.11	1.2	2.23	4.02	1.352	0.1	1.14	99.86
MC-25-1	49.49	19.64	12	0.165	4.82	4.13	1.62	4.57	1.672	0.18	1.9	100.2
Kyanite zone												
MC-4-2	64.38	18.5	5.52	0.062	2.06	0.48	1.09	3.83	0.723	0.07	2.3	99.01
MC-4-3	60.88	14.87	7.68	0.057	5.7	0.95	1.57	4.17	0.891	0.2	1.93	98.89
MC-4-4	61.53	17.73	8.24	0.119	2.96	0.41	0.81	4.2	0.78	0.13	1.95	98.85
MC-4-5	59.1	19.94	8.43	0.105	3.09	0.45	0.93	4.34	0.843	0.11	2.01	99.35
MC-4-6	57.44	23.32	8.58	0.125	2.83	0.52	1.52	2.59	0.795	0.17	1.28	99.17
Sillimanite – K-feldspar zone												
MC-6-6	80.37	10.14	2.7	0.052	0.46	0.68	1.48	2.93	0.448	0.03	0.62	99.9
MC-6-7	71.08	14.79	3.78	0.072	0.83	0.99	2.37	4.69	0.513	0.05	0.93	100.1

Table 4. Whole-rock trace element compositions (in ppm) of the Horsethief Creek Group metasedimentary rocks.

Sample ID	Sc (ppm)	Be	V	Ba	Sr	Y	Zr	Cr	Co	Ni	Cu	Zn	Ga	Ge
Low-grade														
MC-18-1	11	3	62	438	58	33	213	170	11	30	30	170	19	2
MC-31-1	20	2	117	1132	148	21	227	140	21	100	50	120	25	2
MC-31-2	17	2	88	855	111	24	281	130	15	70	40	150	19	2
MC-33-1	16	3	96	871	130	33	187	110	16	60	40	120	29	2
Chlorite zone														
MC-19- 1	14	3	90	539	260	32	233	110	23	50	30	90	25	2
MC-19- 2	11	3	80	510	185	28	207	150	19	50	30	50	20	1
MC- 32- 1	18	3	110	710	95	24	246	120	18	50	30	160	30	2
MC- 32- 2	17	3	94	770	97	18	189	110	21	50	30	150	31	2
Biotite zone														
MC-9- 2	7	1	61	214	225	16	188	60	8	20	< 10	< 30	12	1
MC-9- 3	14	3	88	462	836	33	196	170	13	40	30	90	21	2
MC-9- 4	13	3	79	320	328	37	302	80	13	30	20	< 30	16	1
MC- 27- 1	22	3	145	1220	129	85	603	100	23	50	40	140	28	2
Garnet zone														
MC-9- 1	17	4	114	523	148	34	229	130	16	40	20	80	25	2
MC- 29- 1	12	3	116	732	117	11	331	130	22	40	20	120	22	1
MC- 25- 1	27	3	162	1104	267	48	412	170	30	80	20	180	30	2
Kyanite zone														
MC-4- 2	14	2	97	925	107	22	187	250	5	< 20	20	< 30	23	2
MC-4- 3	14	3	109	585	133	17	218	170	21	90	< 10	90	25	1
MC-4- 4	17	3	102	666	90	31	179	330	15	50	20	80	24	2
MC-4- 5	17	3	108	680	95	33	232	120	17	40	20	90	25	3
MC-4- 6	16	3	113	392	192	25	140	270	20	80	< 10	80	27	2
Sillimanite – K-feldspar zone														
MC-6- 6	7	1	31	744	113	32	380	240	4	< 20	< 10	< 30	12	1
MC-6- 7	10	2	45	1668	286	36	253	40	6	< 20	< 10	30	17	2

Table 4. Continued

As	Rb	Nb	Mo	Ag	In	Sn	Sb	Cs	La	Ce	Pr	Nd	Sm	Eu
7	141	15	2	< 0.5	< 0.2	2	< 0.5	3.8	41.5	86	9.66	37	7.2	1.41
25	130	10	< 2	0.8	< 0.2	3	< 0.5	3.5	69.3	135	14.7	54.6	10.9	2.18
12	97	10	< 2	0.9	< 0.2	2	< 0.5	2.4	55.3	108	11.7	43.7	8.9	1.78
6	189	13	< 2	0.6	< 0.2	3	< 0.5	5.7	96	163	19	68	11.1	2.13
6	133	16	< 2	< 0.5	< 0.2	2	< 0.5	3.7	62.8	128	14.1	52.3	8.8	1.85
< 5	127	11	< 2	< 0.5	< 0.2	1	< 0.5	3.6	43.8	83.4	9.31	33.4	6.1	1.24
11	137	13	< 2	0.8	< 0.2	4	< 0.5	3.3	48.2	104	11	41.8	7.4	1.39
14	154	12	< 2	0.6	< 0.2	4	< 0.5	3.8	48.3	101	10.7	40.7	8.3	1.44
< 5	53	6	< 2	< 0.5	< 0.2	< 1	< 0.5	2.1	23.5	48.9	5.26	19.6	4.1	0.94
< 5	141	15	< 2	< 0.5	< 0.2	3	< 0.5	6.2	51.3	104	11.4	43.5	8.5	1.62
< 5	104	15	< 2	< 0.5	< 0.2	1	< 0.5	4.7	43.7	90.3	9.9	37.6	7.4	1.58
< 5	241	30	< 2	1.7	< 0.2	4	< 0.5	11.4	135	277	30.7	115	22.3	2.92
< 5	143	21	< 2	< 0.5	< 0.2	2	< 0.5	5.5	51.2	107	11.8	43.8	8.5	1.67
< 5	201	16	< 2	0.9	< 0.2	2	< 0.5	5.3	20.1	41.7	4.37	15.6	3.1	0.88
< 5	226	29	< 2	1.3	< 0.2	6	< 0.5	13.6	95.3	191	21.2	79.3	15.3	2.16
< 5	113	12	3	< 0.5	< 0.2	3	< 0.5	2.4	45.5	89.5	9.59	35.5	6.4	1.12
< 5	183	12	< 2	< 0.5	< 0.2	2	< 0.5	6.3	40.4	80	8.69	32.4	6.1	1.21
< 5	168	16	4	< 0.5	< 0.2	3	< 0.5	7.1	57	112	12.4	45.3	8.8	1.74
< 5	173	22	< 2	< 0.5	< 0.2	3	< 0.5	7.5	65.7	131	14.4	52.9	10.2	1.83
< 5	113	14	3	< 0.5	< 0.2	2	< 0.5	4.2	60.3	114	12.5	46.4	8.6	1.94
< 5	94	6	4	0.6	< 0.2	1	< 0.5	2.3	39.7	85.9	9.56	35.7	7	1.16
< 5	167	10	< 2	< 0.5	< 0.2	1	< 0.5	5.4	48.4	102	10.9	39.8	7.9	1.76

Table 4. Continued

Gd	Tb	Dy	Ho	Er	Tm	Yb	Lu	Hf	Ta	W	Tl	Pb	Bi	Th	U
6.7	1	6.3	1.2	3.7	0.56	3.5	0.54	6.1	1.3	< 1	0.3	7	< 0.4	12.5	2.9
7.3	0.9	4.4	0.8	2.3	0.36	2.4	0.4	5.8	0.9	2	0.7	23	< 0.4	20.2	5.2
6.5	0.9	4.7	0.9	2.5	0.38	2.5	0.41	7.4	0.8	2	0.5	9	< 0.4	19.1	7
7.6	1.1	6.5	1.2	3.7	0.52	3.4	0.54	5.1	1.2	1	1	16	< 0.4	21.8	3.1
7.2	1.1	6.1	1.1	3.3	0.48	3	0.48	6.3	1.3	< 1	0.3	19	< 0.4	17.6	3.5
5.6	0.9	5.2	1.1	3.1	0.45	2.9	0.42	5.8	0.9	< 1	0.3	18	< 0.4	13.2	3
5.3	0.8	4.4	0.9	2.6	0.38	2.5	0.4	6.6	1.1	< 1	0.8	24	< 0.4	16.3	3.1
6.1	0.8	4.2	0.8	2.1	0.32	2.1	0.34	4.8	1.1	1	0.9	117	0.5	15.6	2.7
3.7	0.5	3.2	0.6	1.7	0.26	1.7	0.26	4.3	0.9	< 1	< 0.1	12	< 0.4	6.8	1.7
7.1	1.1	6.2	1.2	3.3	0.5	3.3	0.48	5.6	1.4	< 1	0.3	26	< 0.4	15.6	3.2
6.5	1	6.3	1.3	4	0.62	4.2	0.62	8	1.3	< 1	0.2	17	< 0.4	13.9	3
16.9	2.7	16.1	3.1	9.3	1.44	9.8	1.53	15.9	2.2	2	1.4	15	< 0.4	38.3	9.6
7.5	1.2	6.6	1.2	3.6	0.53	3.4	0.54	6.6	1.9	< 1	0.3	19	< 0.4	15.9	3.3
2.5	0.4	2.1	0.4	1.1	0.15	1	0.17	8.6	1.5	1	1.2	9	< 0.4	7.2	1.8
11.5	1.8	9.6	1.8	5	0.72	4.7	0.72	11.6	2.7	3	1.3	24	0.6	30.3	7.7
4.9	0.7	4.1	0.8	2.3	0.33	2.2	0.35	5.1	1.2	< 1	0.2	13	< 0.4	14.5	3.4
5	0.7	3.7	0.7	1.8	0.25	1.6	0.24	5.9	1.2	< 1	0.7	17	< 0.4	12.7	3
7.3	1.1	6.5	1.2	3.6	0.55	3.5	0.52	5.4	1.6	4	0.6	23	< 0.4	17.5	4.5
8.2	1.2	6.9	1.3	3.7	0.55	3.6	0.54	6.5	1.8	< 1	0.6	23	< 0.4	20.3	4.9
7	1	5.4	1	2.7	0.39	2.5	0.35	4.4	1.3	< 1	0.4	39	< 0.4	18.5	4
6	1	5.8	1.2	3.5	0.55	3.7	0.58	9	0.9	2	0.2	17	< 0.4	14.1	3.2
6.5	1.1	6.5	1.3	4.2	0.68	4.6	0.71	7.2	1.2	7	0.5	39	< 0.4	17.4	3.5

Table 5a. Muscovite major-element compositions. Each number is an average of EPMA analyses on three grains, with 1σ value in parentheses.

Sample ID	SiO_2 (wt%)	TiO_2	Al_2O_3	FeO	MnO	MgO	CaO	Na_2O	K_2O	TOTAL
Chlorite zone										
MC-19-1	47.60 (2.33)	0.14 (0.08)	36.91 (2.05)	0.99 (0.63)	0.00 (0.00)	0.65 (0.30)	0.05 (0.06)	1.50 (0.74)	9.00 (0.83)	96.85
Biotite zone										
MC-9-3	47.21 (0.96)	0.37 (0.15)	34.85 (0.39)	1.68 (0.16)	0.01 (0.01)	1.35 (0.11)	0.13 (0.13)	0.22 (0.03)	11.20 (0.22)	97.01
MC-9-4	46.63 (1.09)	0.35 (0.13)	35.46 (0.82)	1.50 (0.25)	0.01 (0.00)	0.94 (0.12)	0.05 (0.10)	0.63 (0.14)	10.50 (0.15)	96.08
Kyanite zone										
MC-4-2	46.07 (0.20)	0.89 (0.07)	35.90 (0.43)	1.05 (0.07)	0.00 (0.00)	0.97 (0.07)	0.00 (0.00)	0.96 (0.02)	9.90 (0.06)	95.74
MC-4-4	46.49 (0.24)	0.91 (0.07)	36.02 (0.71)	1.13 (0.09)	0.00 (0.00)	0.93 (0.11)	0.00 (0.00)	1.00 (0.03)	9.66 (0.07)	96.14
MC-4-5	46.14 (0.17)	0.88 (0.03)	35.90 (0.35)	1.17 (0.09)	0.00 (0.00)	0.98 (0.08)	0.00 (0.00)	1.04 (0.03)	9.79 (0.10)	95.90
MC-4-6	45.90 (0.22)	0.88 (0.06)	35.76 (0.33)	1.15 (0.09)	0.00 (0.00)	0.83 (0.10)	0.00 (0.00)	1.33 (0.05)	9.36 (0.04)	95.21
sillimanite – K-feldspar zone										
MC-6-6	45.54 (0.25)	1.70 (0.19)	35.71 (0.40)	1.42 (0.10)	0.01 (0.00)	0.86 (0.04)	0.00 (0.00)	0.43 (0.04)	10.66 (0.06)	96.31
MC-6-7	45.70 (0.26)	1.72 (0.14)	36.42 (0.53)	1.79 (0.06)	0.01 (0.01)	0.91 (0.05)	0.00 (0.00)	0.40 (0.03)	10.42 (0.10)	97.38

All major element concentrations are reported in weight percent oxide (wt%).

Table 5b. Biotite major-element compositions. Each number is an average of EPMA analyses on three grains, with 1σ value in parentheses.

Sample ID	SiO_2 (wt%)	TiO_2	Al_2O_3	FeO	MnO	MgO	CaO	Na_2O	K_2O	TOTAL
Biotite zone										
MC-9-3	36.16 (0.84)	2.30 (0.37)	18.97 (0.36)	18.78 (0.99)	0.13 (0.01)	10.02 (0.27)	0.05 (0.11)	0.06 (0.02)	9.41 (1.02)	95.89
MC-9-4	36.47 (0.32)	1.94 (0.25)	19.39 (0.43)	18.16 (0.75)	0.10 (0.01)	10.14 (0.32)	0.15 (0.31)	0.14 (0.03)	9.22 (0.28)	95.72
Kyanite zone										
MC-4-2	36.47 (0.35)	2.56 (0.12)	20.50 (0.30)	16.30 (0.26)	0.14 (0.01)	10.57 (0.22)	0.00 (0.00)	0.30 (0.04)	9.10 (0.15)	95.94
MC-4-3	36.80 (0.27)	1.85 (0.05)	20.90 (0.37)	13.78 (0.12)	0.10 (0.01)	12.92 (0.06)	0.00 (0.00)	0.32 (0.03)	9.05 (0.09)	95.72
MC-4-4	36.24 (0.32)	2.30 (0.15)	20.18 (0.24)	18.06 (0.16)	0.13 (0.01)	9.83 (0.15)	0.00 (0.00)	0.31 (0.05)	9.08 (0.09)	96.13
MC-4-5	35.95 (0.31)	2.40 (0.09)	20.16 (0.24)	17.97 (0.14)	0.11 (0.00)	9.52 (0.11)	0.00 (0.00)	0.35 (0.03)	8.93 (0.09)	95.40
MC-4-6	35.86 (0.31)	2.50 (0.08)	20.04 (0.35)	18.29 (0.21)	0.10 (0.01)	9.30 (0.15)	0.00 (0.00)	0.37 (0.04)	8.87 (0.11)	95.33
sillimanite – K-feldspar zone										
MC-6-6	35.45 (0.12)	4.45 (0.18)	19.22 (0.42)	20.68 (0.58)	0.15 (0.01)	6.91 (0.15)	0.00 (0.00)	0.10 (0.02)	9.64 (0.06)	96.61
MC-6-7	35.27 (0.20)	3.99 (0.19)	19.05 (0.22)	20.97 (0.25)	0.23 (0.01)	6.99 (0.12)	0.00 (0.00)	0.10 (0.02)	9.67 (0.07)	96.27

All major element concentrations are reported in weight percent oxide (wt%).

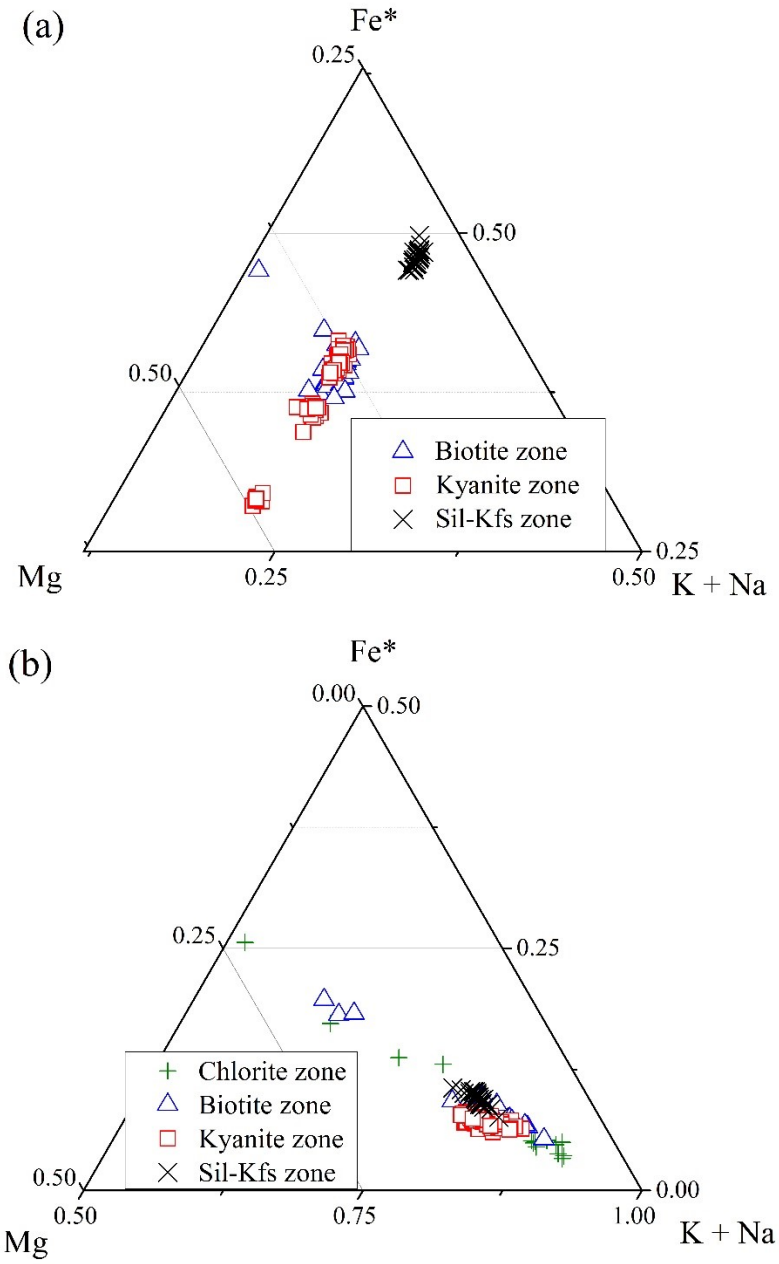

Figure 8. AFM diagram of (a) biotite and (b) muscovite from the Horsethief Creek Group metasedimentary rocks. Fe* is the total iron content. Fe* + Mg + K + Na = 100 mole percent.

5.3 Whole-rock N contents and isotope compositions

The Horsethief Creek Group metasedimentary rocks show large variations in N concentrations and isotope compositions (Table 6). The low-grade slate samples (n = 4) have N contents from 262 to 430 ppm, N/K molar ratios from 20.9 to 43.2, and $\delta^{15}N$ values from 4.1‰ to 6.0‰; the chlorite-zone phyllites (n = 4) have N contents from 244 to 690 ppm, N/K ratios from 19.1 to 64.7, and $\delta^{15}N$ values from 4.2‰ to 5.8‰; the biotite-zone schists (n = 4) contain N contents from 25 to 165 ppm, N/K ratios from 1.7 to 29.1 and $\delta^{15}N$ values from 9.9‰ to 14.8‰; the garnet-zone schists (n = 3) have N contents from 46 to 456 ppm, N/K ratios from 3.8 to 37.4, and $\delta^{15}N$ values from 8.1‰ to 9.6‰; the kyanite-zone schists (n = 6) have N contents from 121 to 304 ppm, N/K ratios from 10.9 to 23.5, and $\delta^{15}N$ values from 7.4‰ to 9.2‰; the Sil-Kfs zone gneisses (n =2) have N contents from 52 to 56 ppm, N/K ratios from 4.0 to 5.9, and $\delta^{15}N$ values from 7.1‰ to 8.1‰. The quartz-feldspar veins in a kyanite zone sample contain 34 ppm N with $\delta^{15}N$ value of 4.2‰.

Table 6. Nitrogen contents and $\delta^{15}N$ values of whole rock samples and mineral separates and their corresponding N/K ratios in the Horsethief Creek Group metasedimentary rocks.

Zone	Sample	Whole rock			Biotite			Muscovite				Plagioclase		K-feldspar	
		N (ppm)	N/K ($\times10^3$)	$\delta^{15}N_{air}$ (‰)	N (ppm)	N/K ($\times10^3$)	$\delta^{15}N_{air}$ (‰)	N* (ppm)	N† (ppm)	N/K ($\times10^3$)	$\delta^{15}N_{air}$ (‰)	N (ppm)	$\delta^{15}N_{air}$ (‰)	N (ppm)	$\delta^{15}N_{air}$ (‰)
Low-grade															
	MC-18-1	262	20.9	5.7											
	MC-31-1	430	43.2	4.1											
	MC-31-2	327	43.4	4.36											
	MC-33-1	298	22.1	6.0											
Chlorite															
	MC-19-1	690	64.7	5.6											
	MC-19-2	472	44.0	4.2											
	MC-32-1	190	19.1	5.8											
	MC-32-2	244	21.9	5.1											
Biotite															
	MC-9-2	66	18.0	10.9	633		11.3								
	MC-9-3	162	15.4	11.2	510	18.2	10.4								
	MC-9-4	165	29.1	9.9	821	29.9	9.4								
	MC-27-1	25	1.7	14.75											
Garnet															
	MC-9-1	456	37.4	8.1	1816	-	8.0								
	MC-25-1	146	10.7	9.5	454	-	9.0								
	MC-29-1	46	3.8	9.6	276	-	8.2								
Kyanite															
	MC-4-1	209	-	8.5											
	MC-4-2	155	13.6	7.7	616	22.7	7.7	261	205 ± 59	8.9	9.5	33	12.9		
	MC-4-3	136	10.9	7.9	667	-	9.4	-	-	-	-	44	7.3		
	MC-4-4	260	20.8	9.2	755	27.9	9.0	260	261 ± 31	9.0	8.7	38	9.4		
	MC-4-5	304	23.5	8.6	845	31.8	8.0	323	299 ± 42	11.1	9.5	29	9		
	MC-4-6	121	15.7	7.4	406	15.4	8.4	169	168 ± 31	6.1	9.0	39	11.7		

Table 5. Continued

Sillimanite – K-feldspar														
MC-6-6	52	5.9	7.1	374	13.0	8.9	158	184 ± 61	5.0	8.67	65	8.8	120	7.7
MC-6-7	56	4.0	8.1	323	11.2	8.2	109	102 ± 33	3.5	9.49	29	7	109	9.1
Quart-feldspar Vein														
MC-V-1	34	-	4.2											

*Nitrogen contents obtained from seal-tube combustion method.

†Nitrogen contents obtained from Fourier-transform infrared spectroscopy (FTIR) method.

5.4 N content and isotopes of mineral separates

Nitrogen concentrations of muscovite in the kyanite and Sil-Kfs zones have been determined by both FTIR and sealed-tube combustion techniques (Table 6). The FTIR method gave a range from 102 to 299 ppm, and the sealed-tube combustion method gave a range from 109 to 323 ppm. These results are well correlated along a line with slope of 1.01 and r^2 of 0.95 (Figure 9). This near one-to-one correlation validates the reliability of both techniques to measure the N contents of minerals.

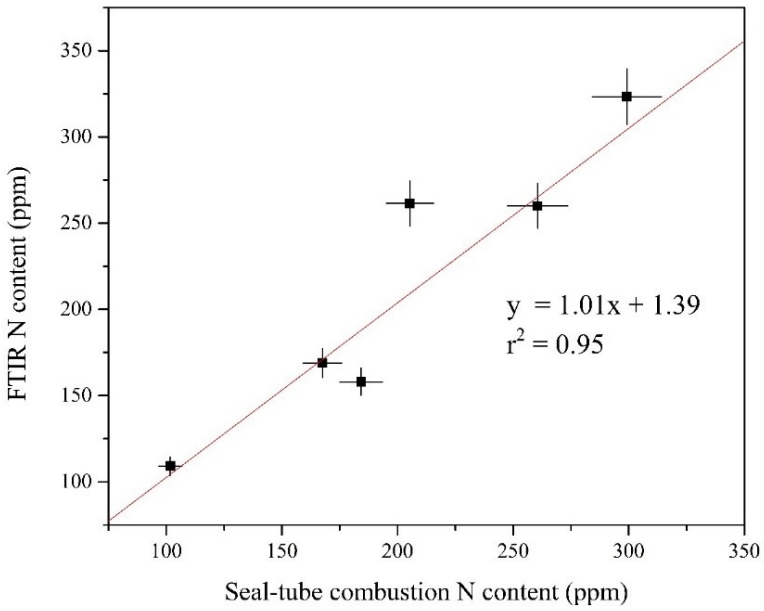

Figure 9. Comparison of N contents of muscovite samples between the Fourier-transform infrared spectroscopy technique and the seal-tube combustion technique. Measurements are made on muscovite grains. The linear fitting yielded a slope of 1.01 and r^2 of 0.95.

Overall, similar to the whole-rock data, mineral separates also show large variations in N concentration and isotope composition. Biotite contains 510 – 821 ppm N with $\delta^{15}N$ of 9.4‰ to 11.3‰ for the biotite zone (average: N = 506 ppm; $\delta^{15}N$ = 10.7‰; n = 4), 276 – 1816 ppm with

$\delta^{15}N$ of 8.0‰ to 9.0‰ for the garnet zone (average: N = 849 ppm; $\delta^{15}N$ = 8.4‰; n = 3), 406 – 845 ppm with $\delta^{15}N$ of 7.7‰ to 9.4‰ for the kyanite zone (average: N = 658 ppm; $\delta^{15}N$ = 8.5‰; n = 5) and 323 – 374 ppm with $\delta^{15}N$ of 8.2‰ to 8.9‰ for the Sil-Kfs zone (average: N = 348 ppm; $\delta^{15}N$ = 8.6‰; n = 2) (Table 5). The N contents and isotope compositions of muscovite show less variability than those of biotite, with the kyanite and Sil-Kfs zone samples range from 169 to 323 ppm with $\delta^{15}N$ from 8.7‰ to 9.5‰ (average: N = 253 ppm; $\delta^{15}N$ = 9.2‰; n = 4), and 109 to 158 ppm with $\delta^{15}N$ from 8.7‰ to 9.5‰ (average: N = 134 ppm; $\delta^{15}N$ = 9.1‰; n = 2), respectively. Plagioclase shows relatively small range of N content from 29 to 44 ppm but large $\delta^{15}N$ variation from 7.3‰ to 12.9‰ for the kyanite zone (average: N = 37 ppm; $\delta^{15}N$ = 10.0‰; n = 5), and 29 to 65 ppm with $\delta^{15}N$ from 7.0‰ to 8.8‰ for the Sil-Kfs zone (average: N = 47 ppm; $\delta^{15}N$ = 7.9‰; n = 2). K-feldspar grains are only found in the Sil-Kfs zone and have N contents from 109 to 120 ppm with $\delta^{15}N$ from 7.7 to 9.1‰ (n = 2). Since K-feldspar minerals are only in one zone, no meaningful conclusion can be reached in this study regarding its variability in N content and isotope composition.

6. Discussion

6.1 Behavior of major and trace elements and whole-rock N during progressive metamorphism

Figure 10 shows ratios of N/K and LOI/Al_2O_3 across the six metamorphic zones in the Mica Creek area. Both indices show consistently high values for the slate and chlorite-zone phyllite, indicating relatively homogeneous volatile components and no significant devolatilization in these two low-grade zones. Starting from the biotite zone, the N/K ratio shows a striking decrease, indicating significant loss of N over K during prograde metamorphism from the chlorite zone to biotite zone. However, the LOI/Al_2O_3 ratio does not show much decrease from the chlorite zone to biotite zone. This may be attributed to addition of volatiles (mostly H_2O) during the retrograde metamorphism of the biotite-zone samples, as evidenced by chlorite distribution along the rim of biotite that can be observed under microscope. Persistent decreasing trends in both LOI/Al_2O_3 the N/K ratios were observed along increasing metamorphic grade from the garnet zone to the Sil-Kfs zone, again suggesting apparently progressive loss of volatiles during prograde metamorphism (Ague, 1994).

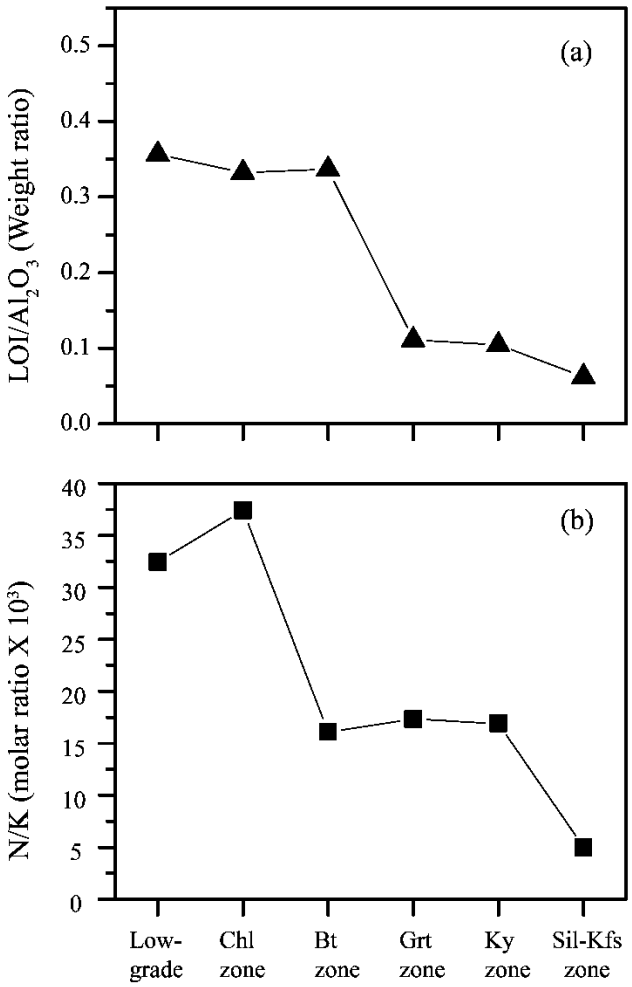

Figure 10. Variations of whole-rock elemental ratios from low- to high-grade rocks in the six metamorphic zones of the Horsethief Creek Group metasedimentary rocks in the Mica Creek area. Chl zone = Chlorite zone; Bt zone = Biotite zone; Grt zone = Garnet zone; Ky zone = Kyanite zone; Sil-Kfs zone = Sillimanite – K-feldspar zone.

To further evaluate the metamorphic devolatilization/dehydration effect on the rocks, we adopted the methodology by Busigny et al. (2003a) by comparing the combined effects on fluid-mobile elements K, Rb and Cs in the metapelites. The model is based on the difference in compatibility between K, Rb and Cs during dehydration reactions, in which Cs is most strongly

fractionated into fluid, followed by Rb and K (Melzer and Wunder, 2000). The systematic changes in K, Rb and Cs abundances following metamorphic devolatilization can be described by Equation 1:

$$R^{f}_{rock} = R^{o}_{rock} \times F^{(1/K_D - 1)} \quad (4)$$

where R^{o}_{rock} and R^{f}_{rock} represent element ratios of fluid-mobile elements (e.g., Rb/K and Rb/Cs) in rocks before and after dehydration, respectively. *F* is the fraction of element remaining in the rock after dehydration. K_D is the ratio of rock-fluid distribution coefficients between Rb-K and Rb-Cs (e.g. $K_D^{Rb-K}{}_{(rock-fluid)} = \frac{R_{Rb}^{rock}/R_K^{rock}}{R_{Rb}^{fluid}/R_K^{fluid}}$).

The modeling is illustrated in Figure 11. In the K versus Rb (Figure 11a) and Rb versus Cs (Figure 11b) diagrams, the data of individual metamorphic grades are scatter but along a broadly linear array. This can be attributed to the heterogeneity in the abundance of K-bearing minerals in rocks in each metamorphic grade. The metamorphic devolatilization effect on the loss of K, Rb, and Cs from the protolith (represented by the low-grade rocks) is marked by the dashed curves. The results show that, in the K vs Rb diagram (Figure 11a), only the biotite-zone data follow the devolatilization trend by showing a decreased slope corresponding to 40% of loss from the overlapped slate and chlorite-zone data. From the garnet zone to the Sil-Kfs zone, the data show an opposite evolving trend. This indicates that at or above garnet zone conditions, metamorphic devolatilization was not the only process operating. An external fluid probably shifted the devolatilization trend. This conclusion is also supported by the Rb vs Cs relationship. On Figure 11b, only chlorite-zone phyllites follow the devolatilization trend with about 2% loss. From biotite zone onward, the data are all shifted away from the devolatilization trend, indicating

that the external fluid even influenced the biotite zone. This may be due to the fact that Cs is more sensitive to fluid.

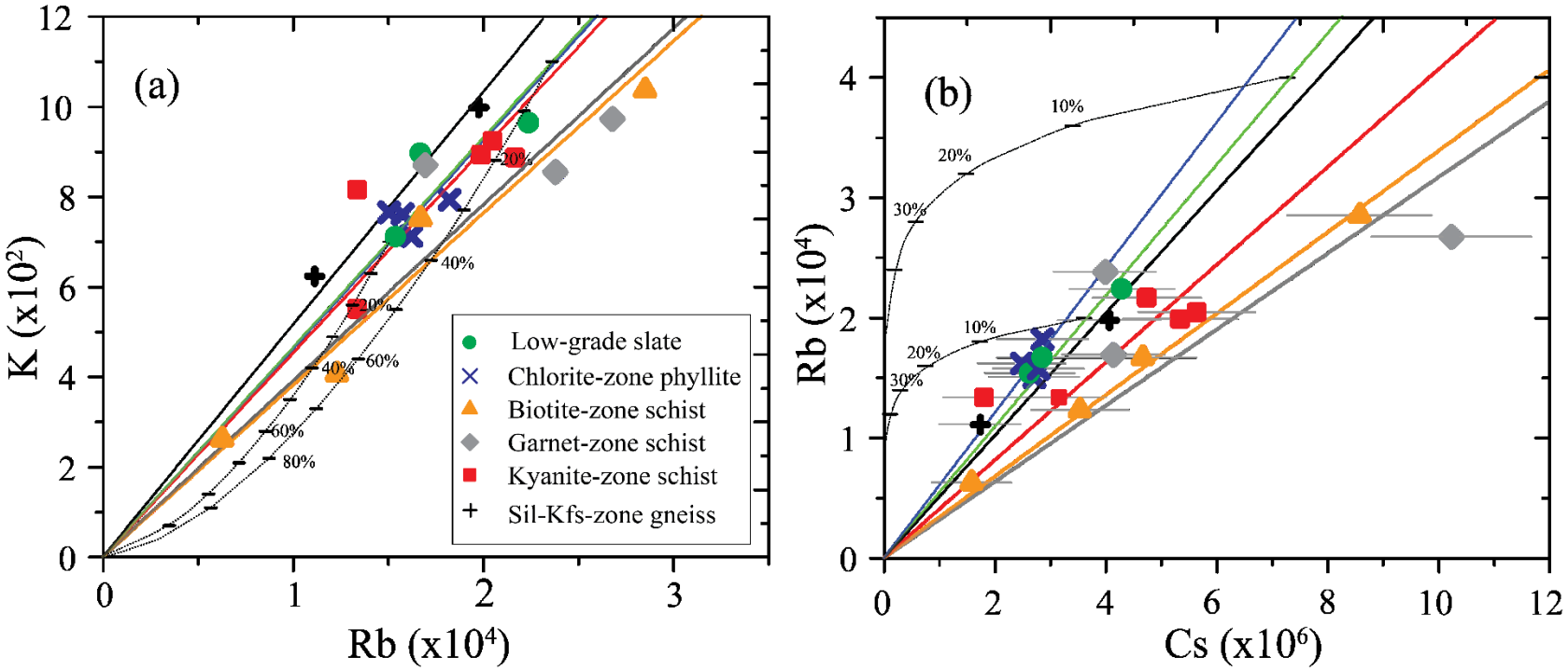

Figure 11. Relationship between K, Rb and Cs (molar abundances) in the Horsethief Creek Group metasedimentary rocks and dehydration modeling. Analytical uncertainty for Cs is shown; analytical uncertainties for Rb and K are smaller than the symbols. The linear fitting of samples in each zone is presented by colored line (low-grade = green; chlorite zone = blue; biotite zone = orange; garnet zone = grey; kyanite zone = red; Sil-Kfs zone = black). Dashed curves represent the evolution path along progressive dehydration from the low-grade line using Eq. 4 and the exchange coefficient data from Busigny et al. (2003a). $\boldsymbol{K_D}$ values corresponding to 600 °C were used. In 11a, the two dashed curves were built from initial K molar abundances of 0.11 and 0.07, respectively; in 11b, the dashed curves were built from initial Rb molar abundances of 0.0004 and 0.0002, respectively. Numbers along the curves mark the fractions of element loss after dehydration.

Since ammonium has very similar ion radius to Rb (1.70Å vs 1.72 Å), how the metamorphic devolatilization and external fluid influenced N in these rocks can be very intriguing. Our results show that the N isotope compositions of the slate- and chlorite-zone samples are relatively uniform ($\delta^{15}N = 5.1 \pm 0.75‰$, n = 8). These values lie within the $\delta^{15}N$ range of sedimentary rocks (2 to 8‰, average ~5.2‰; Li et al., 2014), which mainly reflects the N isotope signature of recycled organic compounds. The consistency in $\delta^{15}N$ values between the low-grade and chlorite-zone samples also agree well with the observation in previous studies of limited shift in $\delta^{15}N$ up to greenschist-facies metamorphism (Rau et al., 1987; Williams et al., 1995; Ader et al., 2006; Busigny and Bebout, 2013). Thus, these two zones can be used to represent the isotopic signature of protolith.

To examine the N response to metamorphic devolatilization and external fluid infiltration, we normalized N concentrations to K concentrations (i.e., N/K ratio) rather than absolute N concentrations as an index. The normalization of N to K is intended to remove the heterogeneity caused by the heterogeneous distribution of N-bearing minerals (mica and feldspar) between samples (see Table 5 or Figure 12)

From low-grade zones to the biotite zone, the samples show a significant decrease in N/K ratio from 20.9 – 43.4 to 1.7 – 29.1 with increase in $\delta^{15}N$ from 4.1 – 6.0‰ to 9.9 – 14.8‰ (Figure 12). This change is consistent with the effect of metamorphic devolatilization reported from previous studies on subduction-zone (Bebout and Fogel, 1992) and collisional orogenic settings (Jia, 2006).

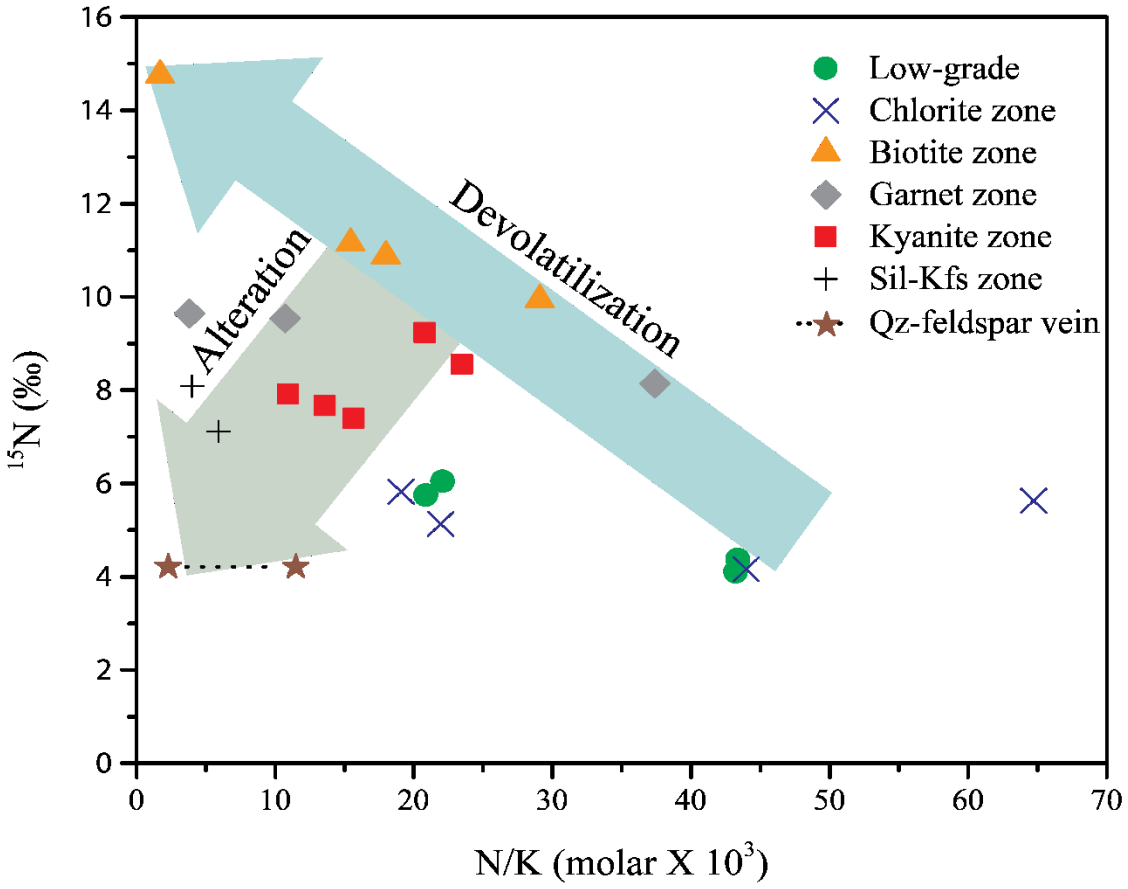

Figure 12. N concentration and δ^{15}N for whole-rock samples of the Horsethief Creek Group metasedimentary rocks. The arrow marked by "Devolatilization" shows the trend of progressive metamorphic loss of N. The arrow marked "Alteration" indicates the trend of alteration by a ^{15}N-depleted granitic melt and its associated fluid. The stars linked by dashed line represent a potential fluid reservoir derived from the quartz-feldspar veins in a kyanite-zone sample with assumed K_2O content in the range of 1 - 5 wt%. See text for discussion.

However, a devolatilization effect on N does not appear to be followed in either garnet, kyanite, or Sil-Kfs zones. In these three metamorphic zones, samples show progressive decreases in both N/K ratios and δ^{15}N values with increasing metamorphic grade (Figure 12). This suggests

that the metamorphic devolatilization effect on N, if there was any, had been overwhelmed by other contemporaneous fluid processes or overprinted by later processes. While the decreases in N/K and N content in garnet, kyanite and Sil-Kfs zones can be explained by the decreasing capacity of silicate minerals to accommodate ammonium with increasing temperature, the decrease in $\delta^{15}N$ values in those zones requires isotope exchange with a ^{15}N-depleted reservoir (Figure 12). One possible candidate for this reservoir is the granitic melt and its associated fluid that precipitate the quartz-feldspar veins found in the kyanite-zone schists. Isotope exchange proceed faster at higher temperature (e.g., for the Sil-Kfs-zone samples) than lower temperature (e.g., for the garnet-zone samples), thus the highest-grade samples have $\delta^{15}N$ values closest to that of the granitic melt, assuming negligible N isotope fractionation between fluid ammonium and mineral (Li, personal communication). One analysis on the whole-rock powder of the veins from a kyanite-zone sample (Figure 3) yielded N content of 34 ppm and $\delta^{15}N$ value of 4.2‰. For the K content of the quartz-feldspar vein, we assume a range of 1 and 5 wt% based on the analyses on veins with similar mineralogy (Sawyer and Robin, 1986; Nabelek, 1997). With that assumption, the N/K ratio would range from 2.3 to 11.5. This melt signature fits well with the expected endmember (Figure 12).

Farquhar (1995) studied the oxygen isotope compositions of quartz, feldspar, muscovite, biotite, garnet and kyanite in the kyanite-zone samples of the Horsethief Creek Group metasedimentary rocks, and found that the $\delta^{18}O$ values of quartz mineral in the kyanite zone were lower than the expected values at equilibrium with garnet and kyanite. He attributed this to a pervasive fluid infiltration event at relatively high-temperature stage, which is partly supported by our N isotopic results – the progressive decreasing trend in N content and isotope composition with increasing metamorphic grade indicates that higher-grade rocks were altered by external

fluid at increasing extents; the lack of overprint on N by external fluid in the biotite zone and lower grades may be attributed to their relatively low temperatures and associated lower N isotope exchange rate between fluid and rock at those temperatures.

Stout et al. (1986) reported considerable amounts of N_2-CH_4 (N_2 mole % > 80%) fluid inclusions in the kyanite-zone samples in the Mica Creek area. These fluid inclusions appear to be a late occurrence because they track cross several grain boundaries. Nevertheless, this later fluid could be an alternative source of N to interact with the metasedimentary rocks. Detailed N isotope composition and fluid temperature conditions are needed to better assess this possibility.

It is worth noting that other isotopic evidence suggests that the gneisses in the Sil-Kfs zone experienced sever retrograde metamorphism. For example, Bowman and Ghent (1986) reported strong deuterium depletion and oxygen isotope disequilibrium among different mineral separates in the Sil-Kfs zone, which have been attributed to the interaction of metapelites with deuterium-depleted meteoric water after peak metamorphism. The trend of decrease in N contents of the Sil-Kfs zone samples (Figures 12) could be partially attributed to the liberation of N during retrograde decomposition of NH_4^+-rich biotite into NH_4^+-poor muscovite (Bos et al., 1988; Mingram and Bräuer, 2001). However, this interpretation cannot be applied to the kyanite zone samples because (1) there is little retrograde metamorphic overprint found in these rocks, and (2) it is not consistent with the $\delta^{15}N$ relationship between biotite and muscovite (see Section 6.3). Thus, it is preferred to explain the decreasing trend in N content and $\delta^{15}N$ value as alteration by ^{15}N-depleted granitic melt and its associated fluid. (Figure 12).

6.2 Fraction of N loss and devolatilized N species during biotite-zone metamorphism

The fraction of N loss during metamorphic devolatilization and the released N speciation have been estimated by numerous previous studies (Bebout and Fogel, 1992; Ague, 1994; Mingram and Bräuer, 2001; Jia, 2006). The main obstacle in the estimation is the heterogeneity in chemical compositions of the protolith. A common way to address this problem is to normalize N to some relatively immobile elements (e.g. Al) (Ague, 1991). For estimating the fraction of N loss, an equation from Ague (1991) is adopted to calculate the mass changes:

$$\tau_i^j = \left[(C_i^0/C_i')(C_j'/C_j^0) - 1\right] \times 100 \quad (5)$$

where τ_i^j is the percentage change in total mass of mobile species *j* relative to immobile species *i*; C_i^0 and C_i' are the initial and final concentrations of immobile species *i*, respectively; C_j^0 and C_j' are the initial and final concentrations of mobile species *j*, respectively. For biotite-zone samples, N should have a generic relationship with Al and K – this is because all N-bearing minerals (clay, micas and feldspars) in this zone contain Al and K and vice versa. Thus, it is reasonable to use Al as a reference to estimate the N loss.

Table 7. Result of calculation of N loss in higher grade rock compared with lower grade samples using the mass balance equation described in Ague (1991) and in text.

Mass loss of N	τ_K^N (%)[a]	τ_{Al}^N (%)[b]	F[c]
Biotite zone	-53	-63	0.47 - 0.37

[a] Calculation of mass loss of N (mobile species) relative to potassium using Eq. 2.

[b] Calculation of mass loss of N (mobile species) relative to aluminium using Eq. 2.

[c] The N fraction remains in the rock after devolatilization.

Since the slate and chlorite-zone phyllite have similar N/K and K/Rb ratios (Figures 11 & 12), they both are considered to resemble the unmetamorphosed equivalent of the Horsethief Creek Group metasedimentary rocks in terms of their N systematics. Table 7 shows that with K and Al as reference frames, we calculate the N loss as 53% and 63% in biotite zone respectively. K is often more mobile than Al and some K may be lost during devolatilization such as those found in the Cooma metamorphic complex (Jia, 2006). Thus, the percentage of N loss estimate made by using K as "immobile element" may be overestimated. Nevertheless, we use these two values as envelop numbers for N loss during the transition from the lowest grade to the biotite zone.

During metamorphic devolatilization, ^{14}N is preferentially lost to the fluid and ^{15}N is enriched in the residue rocks. This can be explained by isotope exchange between ammonium in the rock and the released N species, in form of either NH_3 or N_2 – both have been observed in the step-heating experiments that simulating metamorphic devolatilization process (Scalan, 1958; Haendel et al., 1986). The isotope exchange can be simply expressed as equations below.

$$1/2\,^{15}N\,^{14}N + {}^{14}NH_4^+ \leftrightarrow {}^{15}NH_4^+ + 1/2\,^{14}N_2 \quad (6)$$

$${}^{15}NH_3 + {}^{14}NH_4^+ \leftrightarrow {}^{14}NH_3 + {}^{15}NH_4^+ \quad (7)$$

Two models can be used to describe the ^{15}N shift by metamorphic devolatilization: (1) batch volatilization, in which released N accumulates and remains isotope equilibration with the rock before the accumulated gas is episodically removed out of the system; (2) Rayleigh distillation, in which released N is immediately removed out of the system upon devolatilization and does not interact with the rock (Valley, 1986; Bebout and Fogel, 1992). The equation used to describe the batch volatilization model is

$$\delta^{15}N_f = \delta^{15}N_i - (1-F)1000ln\alpha \quad (8)$$

and the equation used to describe the Rayleigh distillation model is

$$\delta^{15}N_f = \delta^{15}N_i + 1000\left(F^{(\alpha-1)} - 1\right) \quad (9)$$

where $\delta^{15}N_f$ and $\delta^{15}N_i$ are the final and initial N isotope compositions of the rocks, respectively; α is the isotope fractionation factor for either the N_2-NH_4^+ or NH_3-NH_4^+ exchange reaction; F is the fraction of N remaining in the rock after metamorphic devolatilization. Combining the data of N loss and isotopic shift from the low-grade to the biotite-zone samples, possible N species during devolatilization can be identified.

To quantitatively apply these two models, the temperature-dependent N isotope fractionation factors need to be determined first. The temperature of biotite zone in this area is poorly constrained but can be approximated from its metamorphic facies. The temperature of 300 ºC that marks the onset of greenschist facies is considered as the lower limit (Spear, 1993), and a temperature of 500ºC that marks formation of garnet mineral is considered to be the upper boundary for the biotite zone.

Currently, the available N isotope fractionation factors for these two exchange reactions were derived from theoretical calculations (Urey, 1947; Scalan, 1958; Hanschmann, 1981; Petts et al., 2015). But the results vary significantly between different authors. For example, for the temperature range of 300 to 500 ºC, Urey (1947) gave ranges from -9.8‰ to -6.7‰ for Reaction 6 (the N_2-NH_4^+ exchange), and from -14.2‰ to -9.0‰ for Reaction 7 (the NH_3-NH_4^+ exchange), Scalan (1958) gave ranges from -6.1‰ to -4.1‰ for the N_2-NH_4^+ exchange, and from -11.4‰ to -6.9‰ for the NH_3-NH_4^+ exchange, Hanschmann (1981) gave ranges of -4.2‰ to -2.6‰ for the N_2-NH_4^+ exchange, and -12.8‰ to -8.0‰ for the NH_3-NH_4^+ exchange, Petts et al. (2015) gave N

isotope fractionations of -4.3‰ to -3.3‰ for the N_2-NH_4^+ exchange, and -9.8‰ to -6.2‰ for the NH_3-NH_4^+ exchange. Using these isotope fractionation factors, Figure 13 illustrates the range of $\delta^{15}N$ values of the micas from biotite zone with comparison to the results of the N_2-NH_4^+ and NH_3-NH_4^+ isotope exchange results by both batch volatilization and Rayleigh distillation models. The biotite-zone data fit well into both batch volatilization and Rayleigh distillation models (Figure 13e-h) for the NH_3-NH_4^+ pair with fractionation factor obtained from Petts et al. (2015) and Hanschmann (1981), suggesting that N released during biotite-zone metamorphism was in form of NH_3. This observation is consistent with the metasedimentary rocks in the European Variscan Belt, where N release from the greenschist grade rocks was dominated by NH_3 (Mingram and Bräuer, 2001). However, with fractionation factor calculated by Urey (1947) and Scalan (1958), either NH_3 or N_2 could be the N species in the devolatilized fluid.

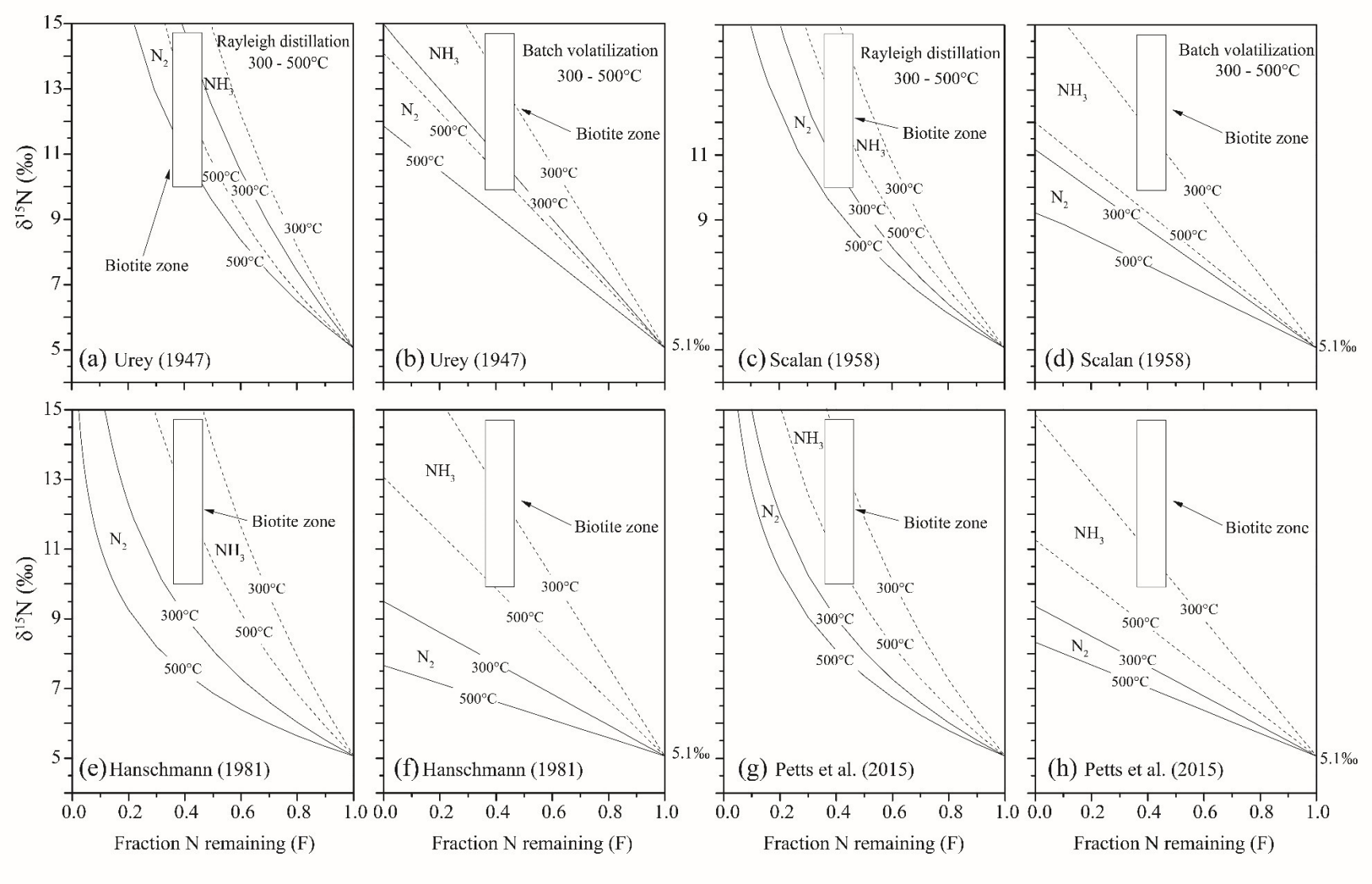

Figure 13. Rayleigh distillation (a,c,e,g) and Batch volatilization models (b,d,f,h) for NH_3-NH_4^+ (dashed lines) and N_2-NH_4^+(solid lines) isotope exchange in the temperature range of 300 – 500ºC. The fractionation factors used are are from Urey (1947) (a and b), Scalan (1958)

(c,d), Hanschmann (1981) (e,f), Petts et al. (2015) (g and h). An initial $\delta^{15}N$ value of +5.1‰ (the average $\delta^{15}N$ value of the low-grade samples) is used. Boxes outline the data of the biotite-zone samples.

6.3 Nitrogen isotope signatures of muscovite, biotite and plagioclase minerals

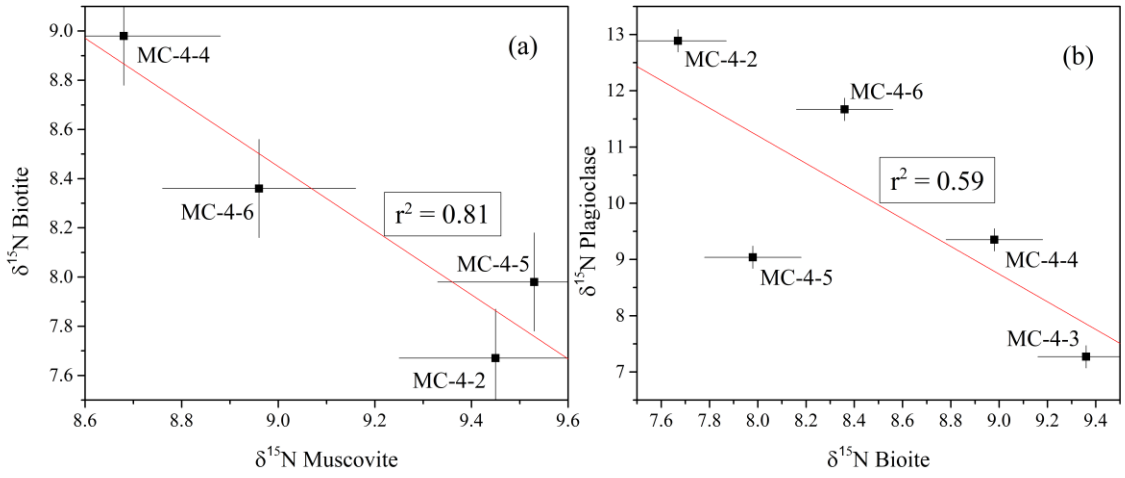

Figure 14. $\delta^{15}N$ values of (a) muscovite and biotite (b) biotite and plagioclase in kyanite zone-samples. Numbers adjacent to symbols are samples IDs. Both $\delta^{15}N$ of Ms-Bt and Bt-Pl pairs give negative correlations. The analytical uncertainties (1σ) for $\delta^{15}N$ of all three minerals are 0.2‰.

Table 8 lists the N partition coefficients (D) of muscovite-biotite and plagioclase-biotite pairs in rocks from the kyanite and Sil-Kfs zones. The ratios show relatively limited variations for both mineral pairs, with average values of 0.38 (1σ = 0.03; n = 6) for muscovite-biotite pair and 0.08 (1σ = 0.04; n = 7) for plagioclase-biotite pair. These values are comparable to previously published N partition coefficients of 0.43 (1σ = 0.11; n = 10) and 0.34 (1σ = 0.06; n = 21) for muscovite-biotite pair, and 0.11 (1σ = 0.04; n = 14) for plagioclase-biotite pair in granitic rocks (Honma and Itihara, 1981; Duit et al., 1986), which suggests that equilibrium partitioning of N between those minerals has been attained at least for the kyanite and Sil-Kfs zones.

Table 8. Distribution coefficients for ammonium in muscovite, biotite and plagioclase.

Sample ID	D (NH4) Mus/Bt	D (NH4) Pl/Bt
Kyanite zone		
Mean ± 1σ	0.38 ± 0.02	0.06 ± 0.02
MC-4-2	0.41	0.05
MC-4-4	0.35	0.05
MC-4-3	-	0.07
MC-4-5	0.38	0.03
MC-4-6	0.38	0.10
Sil-Kfs zone		
Mean ± 1σ	0.37 ± 0.03	0.13 ± 0.04
MC-6-6	0.41	0.17
MC-6-7	0.34	0.09

So far, N isotope fractionations between minerals have been only studied for muscovite-biotite pair through an empirical study (Sadofsky and Bebout, 2000). The results show that, at isotopic equilibrium, there is virtually no N isotope fractionation between muscovite and biotite at 300-700 ºC. This is confirmed by recent theoretical calculations, which suggest that the equilibrium isotope fractionations between muscovite, biotite and K-feldspar are all <0.5‰ at temperatures >150 ºC (Li, personal communication). Plagioclase shows slightly higher $\delta^{15}N$ value (~0.7‰) than the other minerals (Li, personal communication), presumably because the difference in the size of cation site in which NH_4^+ resides (i.e. Na-O distance in plagioclase = 2.80 - 2.81Å; K-O distance in biotite = 2.97Å) (Honma and Itihara, 1981; Sadofsky and Bebout, 2000).

In our samples, although N partitioning between biotite, muscovite and plagioclase reaches apparent equilibration, the difference in $\delta^{15}N$ values between coexisting micas and

feldspars vary significantly (Table 5). For example, muscovite and biotite in MC-4-4 have a $\delta^{15}N$ difference of 0.3‰, which can be considered to be approximately at isotopic equilibrium, whereas those in MC-4-2 show a $\delta^{15}N$ difference up to 1.8‰, indicating obvious isotope disequilibrium between these coexisting minerals.

While there is no systematic change in the major-element concentrations of muscovite and biotite with progressive metamorphism, the kyanite-zone biotite grains show considerable variations in the Fe/Mg ratio (Figure 8). The substitution of Mg^{2+} for Fe^{2+} in biotite can cause major variation in cell parameters which reduces the space between two adjacent octahedral sheets and consequently, the K-O distance (Hazen and Burnham, 1973; Hewitt and Wones, 1975; Duit et al., 1986). Theoretically, a smaller interlayer site would preferentially fractionate the heavier isotope as it forms shorter and stronger bonds. However, there is no correlation between Fe/Mg ratios and $\delta^{15}N$ values of biotite in the kyanite zone (Figure 15), which suggests that the cation exchange may not be the major reason for the observed isotopic disequilibrium.

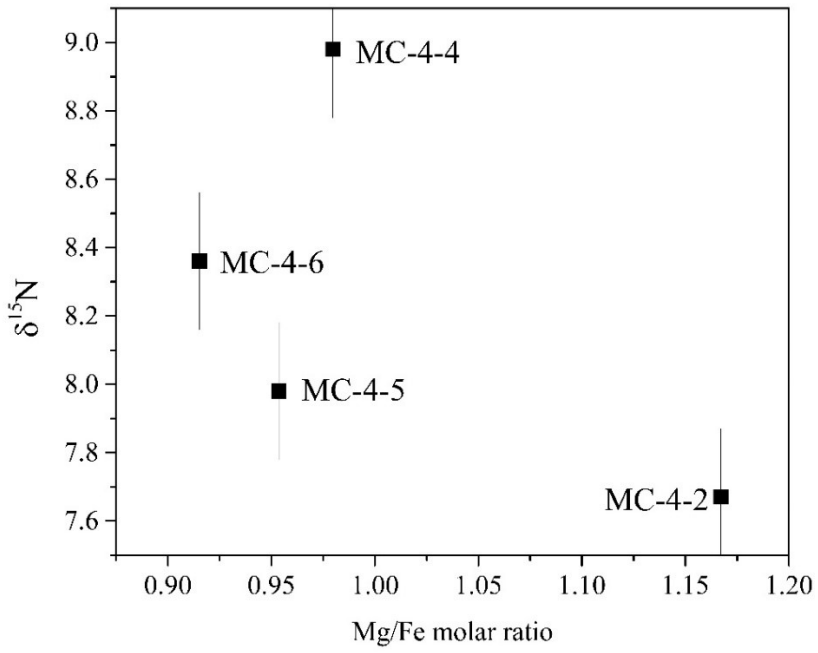

Figure 15. Mg/Fe molar ratio versus N isotope compositions of biotite in the kyanite-zone samples.

It is interesting to note that $\delta^{15}N$ values of both muscovite and plagioclase display a negative relationship with those of biotite in the kyanite-zone samples (Figure 14). Given the facts that these samples were metamorphosed at the same grade and there is no evidence of significant retrograde overprinting, these negative trends are best explained by a kinetic isotopic effect associated with reactions that consumes muscovite and plagioclase to produce biotite. In this process, ^{14}N in muscovite and albite would be used preferentially to synthesize biotite, which causes ^{15}N enrichments in the remaining muscovite and plagioclase and ^{15}N depletion in the biotite product.

So far, a huge number of metamorphic reactions have been proposed for the Barrovian sequence based on petrological studies (Carmichael, 1969; Harte and Hudson, 1979; Pattison and

Tracy, 1991; Whitney et al., 1996; Wei et al., 2004; Prakash et al., 2017). However, very few reactions involve both muscovite and plagioclase in the reactant to produce biotite. Recently, studies on the more comprehensive MnNCKFMASHTO (MnO-Na_2O-CaO-K_2O-FeO-Fe_2O_3-MgO-Al_2O_3-SiO_2-TiO_2-H_2O) system realized that muscovite and plagioclase could both be involved in reactants in the biotite synthesis reactions. For example, Hirsch and Carlson (2006) proposed Reaction 10 for the formation of biotite in the biotite-garnet schist from the Picuris Mountains of New Mexico:

$$Chl + Ms + Ab \rightarrow Bt + Qz + H_2O \quad (10)$$

and Pattison and Spear (2018) proposed Reaction 11 for producing garnet from chlorite:

$$Ms + Chl + Pl + Ilm \rightarrow Grt + Bt + Qz + H_2O \quad (11)$$

Our N isotopic data suggest that plagioclase may be much more involved in metamorphic reactions of a Barrovian sequence than previous thoughts (Ghent et al., 1979; Dempster, 1985; McLellan, 1985). More works on the $\delta^{15}N$ values of minerals in other grades are needed to confirm this idea.

7. Conclusion and Implications

The Neoproterozoic Horsethief Creek Group metasedimentary rocks display a classic Barrovian metamorphic sequence ranging from sub-greenschist to upper amphibolite-facies conditions, and thus provide a natural laboratory to study the behavior of N during regional metamorphism. Our results indicate that the slate and phyllite samples have a relatively small range of $\delta^{15}N$ values despite a large variation of N/K ratio. A significant increase in $\delta^{15}N$ with decreasing N/K ratio occurs when the metamorphic grade increases to the biotite zone, which is consistent with N loss in form of NH_3 by metamorphic devolatilization. With further progressive metamorphism to higher grades, including the garnet zone, kyanite zone and Sil-Kfs zone, although N/K ratios continue to decrease, $\delta^{15}N$ values also decrease, a trend which cannot be explained by metamorphic devolatilization effect. Instead, the trend suggests an overprinting by a ^{15}N-depleted granitic melt and its associated fluid, which was likely the parent fluid of the quartz-feldspar veins observed in the kyanite-zone rocks. In the kyanite-zone samples, N isotope fractionation between muscovite, biotite and plagioclase are at disequilibrium, with a negative relationship in $\delta^{15}N$ between biotite-muscovite pair as well as biotite-plagioclase pair. These relationships can be best explained by a kinetic isotopic effect in a reaction involving muscovite and plagioclase as reactants and biotite as product.

The new data presented here are a valuable addition to the poorly studied N isotope systematics and can help to enhance our understanding of metamorphic devolatilization as well as fluid-rock interactions in an orogenic belt. Previous studies on N behavior during metamorphism have explicitly documented either a pure metamorphic devolatilization effect (i.e., enhanced N loss with increased $\delta^{15}N$ values in higher-grade metamorphic rocks (Haendel et al.,

1986; Bebout and Fogel, 1992; Mingram and Bräuer, 2001; Jia, 2006) or no metamorphic effect (Busigny et al., 2003a; Pitcairn et al., 2005). This present study work in the Horsethief Creek Group metasedimentary rocks illustrates that N isotope behavior can be influenced by more complicated processes in an orogenic belt, including not only metamorphic devolatilization but also fluid alteration. In turn, this study also demonstrates the effectiveness of N isotopes as a tracer for probing a variety of geochemical processes in a complicated geological system.

In addition, this thesis also explored some new directions in N isotope studies. Stepping forward from previous studies on metamorphic rocks that mostly focused on whole-rock analysis, I also examined N isotopic signatures of mineral separates. In particular, to my knowledge, this thesis produced the first batch of N isotope data for plagioclase and K-feldspar. Integration of these mineral data may provide new insights into metamorphic reactions that cannot be easily identified by conventional petrological analysis.

8. Future Work

The study of N systematic has primarily focused on whole rock analysis, whereas N isotopic compositions of individual minerals that are sensitive to different geological processes are poorly known. The equilibrium or disequilibrium isotopic fractionations between coexisting minerals can provide valuable information such as fluid-rock interaction, endmember mixing, but simply cannot be attained from the whole rock analysis. The present study observed $\delta^{15}N$ correlation between muscovite, biotite and plagioclase, which have never been seen before. More mineral separates should be collected from other zones to test the theory. In addition, minor alteration of biotite has been found in some of our samples, and its influence on N isotope composition is still poorly understood. Boyd and Philippot (1998) reported that the $\delta^{15}N$ difference between biotite and muscovite is very small even in the most altered samples. However, according to Bos et al. (1988), N_2 can be easily released when biotite is altered to form chlorite or white mica during retrograde metamorphism, in which there should be fractionations in a magnitude detectable by the modern N isotope analytical techniques. Plessen et al. (2010) showed that a significant negative shift in $\delta^{15}N$ values of biotite grains from the lowest grade to staurolite zone, which is tentatively explained by retrograde metamorphic overprinting on the lower grade rocks. More detailed studies on the behavior of N isotopes in response to different geological processes should be examined in detail in the future in order to effectively use N isotopes as a trace for probing metamorphic and igneous processes.

9. Reference

Ader, M., Boudou, J.-P., Javoy, M., Goffé, B. and Daniels, E. (1998) Isotope study on organic nitrogen of Westphalian anthracites from the Western Middle field of Pennsylvania (USA) and from the Bramsche Massif (Germany). Organic Geochemistry 29, 315-323.

Ader, M., Cartigny, P., Boudou, J.-P., Oh, J.-H., Petit, E. and Javoy, M. (2006) Nitrogen isotopic evolution of carbonaceous matter during metamorphism: Methodology and preliminary results. Chemical Geology 232, 152-169.

Ague, J.J. (1991) Evidence for major mass transfer and volume strain during regional metamorphism of pelites. Geology 19, 855-858.

Ague, J.J. (1994) Mass transfer during Barrovian metamorphism of pelites, south-central Connecticut; I, Evidence for changes in composition and volume. American Journal of Science 294, 989-1057.

Barker, D.S. (1964) Ammonium in alkali feldspars. American Mineralogist: Journal of Earth and Planetary Materials 49, 851-858.

Bebout, G.E. (1997) Nitrogen isotope tracers of high-temperature fluid-rock interactions: Case study of the Catalina Schist, California. Earth and Planetary Science Letters 151, 77-90.

Bebout, G.E. and Fogel, M.L. (1992) Nitrogen-isotope compositions of metasedimentary rocks in the Catalina Schist, California: implications for metamorphic devolatilization history. Geochimica et Cosmochimica Acta 56, 2839-2849.

Bebout, G.E., Idleman, B.D., Li, L. and Hilkert, A. (2007) Isotope-ratio-monitoring gas chromatography methods for high-precision isotopic analysis of nanomole quantities of silicate nitrogen. Chemical Geology 240, 1-10.

Bos, A., Duit, W., van der Eerden, A.M. and Jansen, J.B.H. (1988) Nitrogen storage in biotite: An experimental study of the ammonium and potassium partitioning between 1M-phlogopite and vapour at 2 kb. Geochimica et Cosmochimica Acta 52, 1275-1283.

Bowman, J. and Ghent, E. (1986) Oxygen and hydrogen isotope study of minerals from metapelitic rocks, staurolite to sillimanite zones, Mica Creek, British Columbia. Journal of Metamorphic Geology 4, 131-141.

Boyd, S.R. and Philippot, P. (1998) Precambrian ammonium biogeochemistry: a study of the Moine metasediments, Scotland. Chemical Geology 144, 257-268.

Busigny, V. and Bebout, G.E. (2013) Nitrogen in the silicate Earth: Speciation and isotopic behavior during mineral–fluid interactions. Elements 9, 353-358.

Busigny, V., Cartigny, P., Philippot, P., Ader, M. and Javoy, M. (2003a) Massive recycling of nitrogen and other fluid-mobile elements (K, Rb, Cs, H) in a cold slab environment: evidence from HP to UHP oceanic metasediments of the Schistes Lustrés nappe (western Alps, Europe). Earth and Planetary Science Letters 215, 27-42.

Busigny, V., Cartigny, P., Philippot, P. and Javoy, M. (2003b) Ammonium quantification in muscovite by infrared spectroscopy. Chemical Geology 198, 21-31.

Carmichael, D.M. (1969) On the mechanism of prograde metamorphic reactions in quartz-bearing pelitic rocks. Contributions to Mineralogy and Petrology 20, 244-267.

Carmichael, D.M. (1978) Metamorphic bathozones and bathograds; a measure of the depth of post-metamorphic uplift and erosion on the regional scale. American Journal of Science 278, 769-797.

Craw, D. (1978) Metamorphism, structure and stratigraphy in the southern Park Ranges, British Columbia. Canadian Journal of Earth Sciences 15, 86-98.

Crowley, J., Ghent, E., Carr, S., Simony, P. and Hamilton, M. (2000) Multiple thermotectonic events in a continuous metamorphic sequence, Mica Creek area, southeastern Canadian Cordillera. Geological Materials Research 2, 1-46.

Darimont, A., Burke, E. and Touret, J. (1988) Nitrogen-rich metamorphic fluids in Devonian metasediments from Bastogne, Belgium. Bulletin de minéralogie 111, 321-330.

Dempster, T. (1985) Garnet zoning and metamorphism of the Barrovian type area, Scotland. Contributions to Mineralogy and Petrology 89, 30-38.

Dickinson, W.R. (1976) Sedimentary basins developed during evolution of Mesozoic–Cenozoic arc–trench system in western North America. Canadian Journal of Earth Sciences 13, 1268-1287.

Digel, S.G., Ghent, E.D., Carr, S.D. and Simony, P.S. (1998) Early Cretaceous kyanite-sillimanite metamorphism and Paleocene sillimanite overprint near Mount Cheadle, southeastern British Columbia: Geometry, geochronology, and metamorphic implications. Canadian Journal of Earth Sciences 35, 1070-1087.

Duit, W., Jansen, J.B.H., van Breemen, A. and Bos, A. (1986) Ammonium micas in metamorphic rocks as exemplified by Dome de l'Agout (France). American Journal of Science 286, 702-732.

Farquhar, J. (1995) Strategies for high-temperature oxygen isotope thermometry. University of Alberta, p. 184.

Ferry, J.M. (1988) Infiltration-driven metamorphism in northern New England, USA. Journal of Petrology 29, 1121-1159.

Ferry, J.M. and Spear, F. (1978) Experimental calibration of the partitioning of Fe and Mg between biotite and garnet. Contributions to Mineralogy and Petrology 66, 113-117.

Ghent, E. and Valley, J. (1998) Oxygen isotope study of quartz-Al2SiO5 pairs from the Mica Creek area, British Columbia: implications for the recovery of peak metamorphic temperatures. Journal of Metamorphic Geology 16, 223-230.

Ghent, E.D. and Gordon, T.M. (2000) Application of INVEQ to the geothermobarometry of metamorphic rocks near a kyanite-sillimanite isograd, Mica Creek, British Columbia. American Mineralogist 85, 9-13.

Ghent, E.D., Nicholls, J., Stout, M.Z. and Rottenfusser, B. (1977) Clinopyroxene amphibolite boudins from Three Valley Gap, British Columbia. The Canadian Mineralogist 15, 269-282.

Ghent, E.D., Robbins, D.B. and Stout, M.Z. (1979) Geothermometry, geobarometry, and fluid compositions of metamorphosed calc-silicates and pelites, Mica Creek, British Columbia. American Mineralogist 64, 874-885.

Ghent, E.D., Simony, P.S. and Knitter, C.C. (1980) Geometry and pressure-temperature significance of the kyanite-sillimanite isograd in the Mica Creek area, British Columbia. Contributions to Mineralogy and Petrology 74, 67-73.

Haendel, D., Mühle, K., Nitzsche, H.-M., Stiehl, G. and Wand, U. (1986) Isotopic variations of the fixed nitrogen in metamorphic rocks. Geochimica et Cosmochimica Acta 50, 749-758.

Halama, R., Bebout, G.E., Marschall, H.R. and John, T. (2017) Fluid-induced breakdown of white mica controls nitrogen transfer during fluid–rock interaction in subduction zones. International Geology Review 59, 702-720.

Hanschmann, G. (1981) Berechnung von isotopieeffekten auf quantenchemischer grundlage am beispiel stickstoffhaltiger molecule. Zfl-Mitt 41, 19-31.

Harte, B. and Hudson, N.F. (1979) Pelite facies series and the temperatures and pressures of Dalradian metamorphism in E Scotland. Geological Society, London, Special Publications 8, 323-337.

Hazen, R.M. and Burnham, C.W. (1973) The crystal structures of one-layer phlogopite and annite. American Mineralogist 58, 889-900.

Hewitt, D.A. and Wones, D.R. (1975) Physical properties of some synthetic Fe-Mg-Al trioctahedral biotites. American Mineralogist: Journal of Earth and Planetary Materials 60, 854-862.

Hirsch, D. and Carlson, W. (2006) Variations in rates of nucleation and growth of biotite porphyroblasts. Journal of Metamorphic Geology 24, 763-777.

Honma, H. and Itihara, Y. (1981) Distribution of ammonium in minerals of metamorphic and granitic rocks. Geochimica et Cosmochimica Acta 45, 983-988.

Jia, Y. (2006) Nitrogen isotope fractionations during progressive metamorphism: A case study from the Paleozoic Cooma metasedimentary complex, southeastern Australia. Geochimica et Cosmochimica Acta 70, 5201-5214.

Jia, Y. and Kerrich, R. (1999) Nitrogen isotope systematics of mesothermal lode gold deposits: Metamorphic, granitic, meteoric water, or mantle origin? Geology 27, 1051-1054.

Li, L., Bebout, G.E. and Idleman, B.D. (2007) Nitrogen concentration and δ 15 N of altered oceanic crust obtained on ODP Legs 129 and 185: insights into alteration-related nitrogen enrichment and the nitrogen subduction budget. Geochimica et Cosmochimica Acta 71, 2344-2360.

Li, L., Zheng, Y.-F., Cartigny, P. and Li, J. (2014) Anomalous nitrogen isotopes in ultrahigh-pressure metamorphic rocks from the Sulu orogenic belt: Effect of abiotic nitrogen reduction during fluid–rock interaction. Earth and Planetary Science Letters 403, 67-78.

McLellan, E. (1985) Metamorphic reactions in the kyanite and sillimanite zones of the Barrovian type area. Journal of Petrology 26, 789-818.

Melzer, S. and Wunder, B. (2000) Island-arc basalt alkali ratios: Constraints from phengite-fluid partitioning experiments. Geology 28, 583-586.

Mikhail, S. and Sverjensky, D.A. (2014) Nitrogen speciation in upper mantle fluids and the origin of Earth's nitrogen-rich atmosphere. Nature Geoscience 7, 816.

Mingram, B. and Bräuer, K. (2001) Ammonium concentration and nitrogen isotope composition in metasedimentary rocks from different tectonometamorphic units of the European Variscan Belt. Geochimica et Cosmochimica Acta 65, 273-287.

Monger, J. and Price, R. (2002) The Canadian Cordillera: geology and tectonic evolution. CSEG Recorder 27, 17-36.

Monger, J., Price, R. and Tempelman-Kluit, D. (1982) Tectonic accretion and the origin of the two major metamorphic and plutonic welts in the Canadian Cordillera. Geology 10, 70-75.

Monger, J., Souther, J. and Gabrielse, H. (1972) Evolution of the Canadian Cordillera; a plate-tectonic model. American Journal of Science 272, 577-602.

Nabelek, P.I. (1997) Quartz-sillimanite leucosomes in high-grade schists, Black Hills, South Dakota: A perspective on the mobility of Al in high-grade metamorphic rocks. Geology 25, 995-998.

Pattison, D.R. and Spear, F.S. (2018) Kinetic control of staurolite–Al2SiO5 mineral assemblages: Implications for Barrovian and Buchan metamorphism. Journal of Metamorphic Geology.

Pattison, D.R. and Tracy, R.J. (1991) Phase equilibria and thermobarometry of metapelites. Reviews in Mineralogy and Geochemistry 26, 105-206.

Petts, D., Chacko, T., Stachel, T., Stern, R. and Heaman, L. (2015) A nitrogen isotope fractionation factor between diamond and its parental fluid derived from detailed SIMS analysis of a gem diamond and theoretical calculations. Chemical Geology 410, 188-200.

Pitcairn, I.K., Teagle, D.A., Kerrich, R., Craw, D. and Brewer, T.S. (2005) The behavior of nitrogen and nitrogen isotopes during metamorphism and mineralization: evidence from the Otago and Alpine Schists, New Zealand. Earth and Planetary Science Letters 233, 229-246.

Plessen, B., Harlov, D.E., Henry, D. and Guidotti, C.V. (2010) Ammonium loss and nitrogen isotopic fractionation in biotite as a function of metamorphic grade in metapelites from western Maine, USA. Geochimica et Cosmochimica Acta 74, 4759-4771.

Prakash, D., Patel, D.K., Tewari, S., Yadav, M.K. and Yadav, R. (2017) Metamorphic zonal sequences of pelitic schists and gneisses from the area around Kandra (Jharkhand): Constraints from field and textural relationship. Journal of the Geological Society of India 89, 139-144.

Raeside, R.P. and Simony, P.S. (1983) Stratigraphy and deformational history of the Scrip nappe, Monashee Mountains, British Columbia. Canadian Journal of Earth Sciences 20, 639-650.

Rau, G.H., Arthur, M.A. and Dean, W.E. (1987) 15N/14N variations in Cretaceous Atlantic sedimentary sequences: implication for past changes in marine nitrogen biogeochemistry. Earth and Planetary Science Letters 82, 269-279.

Rye, R.O., Schuiling, R.D., Rye, D.M. and Jansen, J.B.H. (1976) Carbon, hydrogen, and oxygen isotope studies of the regional metamorphic complex at Naxos, Greece. Geochimica et Cosmochimica Acta 40, 1031-1049.

Sadofsky, S.J. and Bebout, G.E. (2000) Ammonium partitioning and nitrogen-isotope fractionation among coexisting micas during high-temperature fluid-rock interactions: Examples from the New England Appalachians. Geochimica et Cosmochimica Acta 64, 2835-2849.

Sawyer, E. and Robin, P.Y. (1986) The subsolidus segregation of layer-parallel quartz-feldspar veins in greenschist to upper amphibolite facies metasediments. Journal of Metamorphic Geology 4, 237-260.

Scalan, R.S. (1958) The isotopic composition, concentration, and chemical state of the nitrogen in igneous rocks. University of Arkansas, Fayetteville.

Sigman, D., Karsh, K. and Casciotti, K. (2009) Ocean process tracers: nitrogen isotopes in the ocean.

Simony, P., Ghent, E., Craw, D., Mitchell, W. and Robbins, D. (1980) Structural and metamorphic evolution of northeast flank of Shuswap complex.

Spear, F.S. (1993) Metamorphic phase equilibria and pressure-temperature-time paths. Mineralogical Society of America Washington, DC.

Stevenson, F. (1959) On the presence of fixed ammonium in rocks. Science 130, 221-222.

Stevenson, F. (1962) Chemical state of the nitrogen in rocks. Geochimica et Cosmochimica Acta 26, 797-809.

Stout, M., Crawford, M. and Ghent, E. (1986) Pressure-temperature and evolution of fluid compositions of Al 2 SiO 5-bearing rocks, Mica Creek, BC, in light of fluid inclusion data and mineral equilibria. Contributions to Mineralogy and Petrology 92, 236-247.

Tinkham, D.K. and Ghent, E.D. (2005) Estimating PT conditions of garnet growth with isochemical phase-diagram sections and the problem of effective bulk-composition. The Canadian Mineralogist 43, 35-50.

Urey, H.C. (1947) The thermodynamic properties of isotopic substances. Journal of the Chemical Society 562-581.

Valley, J.W. (1986) Stable isotope geochemistry of metamorphic rocks. Reviews in Mineralogy 16, 445-489.

Wei, C., Powell, R. and Clarke, G. (2004) Calculated phase equilibria for low-and medium-pressure metapelites in the KFMASH and KMnFMASH systems. Journal of Metamorphic Geology 22, 495-508.

Whitney, D., Mechum, T., Kuehner, S. and Dilek, Y. (1996) Progressive metamorphism of pelitic rocks from protolith to granulite facies, Dutchess County, New York, USA: constraints on the timing of fluid infiltration during regional metamorphism. Journal of Metamorphic Geology 14, 163-181.

Whitney, D.L. and Evans, B.W. (2010) Abbreviations for names of rock-forming minerals. American Mineralogist 95, 185-187.

Williams, L.B., Ferrell Jr, R.E., Hutcheon, I., Bakel, A.J., Walsh, M.M. and Krouse, H.R. (1995) Nitrogen isotope geochemistry of organic matter and minerals during diagenesis and hydrocarbon migration. Geochimica et Cosmochimica Acta 59, 765-779.

Yamamoto, T. and Nakahira, M. (1966) Ammonium ions in sericites. American Mineralogist: Journal of Earth and Planetary Materials 51, 1775-1778.

Yui, T.-F., Kao, S.-J. and Wu, T.-W. (2009) Nitrogen and N-isotope variation during low-grade metamorphism of the Taiwan mountain belt. Geochemical Journal 43, 15-27.

Appendix

The GPS coordinates of Sampling locations are listed below:

Sample Number	GPS coordinates
Slate	
MC-18-1	N:51º21'17.5", W:117º26'16.8"
MC-31-1	N:51º21'29.2", W:117º26'17.1"
MC-31-2	
MC-33-1	N:51º31'32.2", W:117º25'54.9"
Chlorite zone	
MC-19-1	N:51º30'22.6", W:117º26'55.5"
MC-19-2	
MC-32-1	N:51º30'50.8", W:117º25'43.2"
MC-32-2	
Biotite zone	
MC-9-2	N:51º49'20.6", W:118º38'28.6"
MC-9-3	
MC-9-4	N:51º49'20.2", W:118º38'28.2"
Mc-27-1	N:52º03'44.2", W:118º34'08.6"
Garnet zone	
MC-9-1	N:51º49'20.6", W:118º38'28.6"
MC-25-1	N:52º04'48.2", W:118º33'33.2"
MC-29-1	N:52º01'55.4", W:118º34'59.8"
Kyanite zone	
MC-4-1	N:52º05'33", W:118º31'48.6"
MC-4-2	
MC-4-3	
MC-4-4	
MC-4-5	
MC-4-6	
Sil-Kfs zone	
MC-6-6	N:51º58'12.3", W:118º33'34.8"
MC-6-7	N:51º58'12.1", W:118º33'34.8"